Naval Research Laboratory

Washington, DC 20375-5320

NRL/MR/6709--97-7960

Quasineutral Particle Simulation of Magnetized Plasma Discharges: General Formalism and Application to ECR Discharges

MARTIN LAMPE
GLENN JOYCE
WALLACE M. MANHEIMER
STEVEN P. SLINKER

Plasma Physics Division

July 31, 1997

REPORT DOCUMENTATION PAGE

Form Approved
OMB No. 0704-0188

1. AGENCY USE ONLY (*Leave Blank*)	2. REPORT DATE	3. REPORT TYPE AND DATES COVERED
	July 31, 1997	Interim

4. TITLE AND SUBTITLE

Quasineutral Particle Simulation of Magnetized Plasma Discharges: General Formalism and Application to ECR Discharges

5. FUNDING NUMBERS

JO# 67-5738-0-7

6. AUTHOR(S)

Martin Lampe, Glenn Joyce, Wallace M. Manheimer, and Steven P. Slinker

7. PERFORMING ORGANIZATION NAME(S) AND ADDRESS(ES)

Naval Research Laboratory
Washington, DC 20375-5320

8. PERFORMING ORGANIZATION REPORT NUMBER

NRL/MR/6709--97-7960

9. SPONSORING/MONITORING AGENCY NAME(S) AND ADDRESS(ES)

Office of Naval Research
Arlington, VA 22217

10. SPONSORING/MONITORING AGENCY REPORT NUMBER

11. SUPPLEMENTARY NOTES

12a. DISTRIBUTION/AVAILABILITY STATEMENT

Approved for public release; distribution unlimited.

12b. DISTRIBUTION CODE

13. ABSTRACT (*Maximum 200 words*)

In quasineutral plasmas it is difficult and inefficient to calculate the electrostatic field from Poisson's equation. We have developed a particle-in-cell/Monte Carlo (PIC/MC) simulation method for magnetized discharges, in which internal electric fields and sheath potentials are determined directly from the requirement of quasineutrality. Sheaths are treated as thin potential barriers, and the Bohm criterion for ion flux into the sheath is imposed as a boundary condition. Electron plasma oscillations do not appear in the model, and the Debye length is essentially set to zero. Thus time steps and spatial gridding can be chosen to represent the macroscopic time and space scales of interest, greatly enhancing numerical efficiency. The simulation technique correctly represents kinetic features such as Landau damping. We believe it is applicable generally to a wide variety of phenomena in plasmas that may be magnetized or unmagnetized, bounded or unbounded, collisional or collisionless. We present results from an axisymmetric simulation of an electron cyclotron resonance (ECR) discharge in low-pressure argon, which show that the discharge is strongly affected by cross-field ion flows, even when the vessel walls are insulators. We also present analytic calculations based on the model, which afford new insights into cross-field transport in a metallic vessel, and show that the classic Simon diffusion can be strongly inhibited by the effect of sheath potentials.

14. SUBJECT TERMS

Particle simulation
Quasineutral plasma
Plasma processing
Electronic cyclotron resonance plasma source
Plasma simulation

15. NUMBER OF PAGES

52

16. PRICE CODE

17. SECURITY CLASSIFICATION OF REPORT	18. SECURITY CLASSIFICATION OF THIS PAGE	19. SECURITY CLASSIFICATION OF ABSTRACT	20. LIMITATION OF ABSTRACT
UNCLASSIFIED	UNCLASSIFIED	UNCLASSIFIED	UL

NSN 7540-01-280-5500

Standard Form 298 (Rev. 2-89)
Prescribed by ANSI Std 239-18
298-102

CONTENTS

QUASINEUTRAL PARTICLE SIMULATION OF MAGNETIZED PLASMA DISCHARGES: GENERAL FORMALISM AND APPLICATION TO ECR DISCHARGES

1. Introduction

In recent years, there has been considerable interest in the use of low pressure, high density plasma sources for materials processing, e.g. for semiconductor etching, and also for some types of chemical vapor deposition.[1] These types of sources, which include electron cyclotron resonance (ECR), helicon and inductively-coupled sources, operate at gas pressure ranging from 10 mTorr to below 1 mTorr, and plasma density from several $\times 10^{11}$ to 10^{13} cm^{-3}. In this regime, fluid models are not well matched to the characteristics of either the ions or the electrons. For example, mean free paths can be comparable to device dimensions, the electron response to the driving electromagnetic fields can be nonlocal, and velocity distribution functions can be non-Maxwellian (particularly for the high energy electrons that determine sheath potentials, ionization rates, and other inelastic collisional processes). For these reasons, fully kinetic simulation models are needed to properly represent the overall physics and chemistry of the discharge.

A natural approach to modeling of these types of discharges is the use of particle-in-cell (PIC) computer simulations which also include a Monte Carlo (MC) representation of collisional processes (PIC/MC models).[2] In these simulations, the motion of particles between collisions is followed deterministically, under the influence of specified external magnetic fields, and self-consistent electrostatic fields computed by calculating the charge density of the particles and then solving Poisson's equation. Recent years have seen major advances in the development and use of PIC/MC codes.[2-11] In most cases, the objective of a simulation is to calculate the characteristics of the plasma steady state, or at most of a slowly varying state, as a function of the machine control parameters. However, the enormous range of spatial and temporal scales in a high-density discharge precludes straightforward application of the PIC/MC procedure to simulations of the entire discharge. As an example, the spatial and temporal scales for a typical ECR plasma are summarized in Table 1. With respect to plasma transport and electrical properties, the approach to a steady state occurs over time scales characterized by the escape of ions to the walls, which are typically on the order of 0.1 ms to several ms. The evolution to a steady state of the chemistry may occur on an even longer time scale characterized by the residence of neutrals

Manuscript approved June 11, 1997.

in the system. However, a straightforward PIC code must resolve all of the shorter time scales, down to and including the electron plasma frequency, electron gyrofrequency and microwave frequency time scales, which are on the order of picoseconds. Similarly, the spatial scales of real interest in a reactor-scale simulation are macroscopic scale lengths (centimeters), but a straightforward particle simulation would have to resolve a vast range of spatial scales, down to the electron gyroradius, the Debye length, and the thickness of passive sheaths, which are typically 0.01 to 0.1 cm. It would be essentially impossible, even with a supercomputer, to resolve this range of spatial and temporal scales within a multi-dimensional simulation. To the greatest extent possible, one would like to simulate the macroscopic features and the approach to equilibrium, while excluding the fast time scales and short spatial scales from the simulation.

One approach to the problem of time scale diversity is the use of implicit coding to avoid resolution of the electron plasma frequency time scale.[12-17] However, PIC simulation techniques also face a more fundamental difficulty arising from the circumstances of quasineutrality. The internal electrostatic field within the bulk plasma plays an essential role in the transport of plasma toward the walls, and therefore strongly influences the overall structure and characteristics of the discharge. This field is typically less than 1 V/cm in the central plasma, up to a few V/cm in the presheath. When viewed in the light of Poisson's equation,

$$\nabla^2\phi = 4\pi e(n_e - n_i), \tag{1}$$

the source of this field, $n_i - n_e$, represents an electron-ion charge separation that is less than 10^{-5} of the density of either electrons or ions. This type of situation is actually quite common throughout plasma physics, as processes occurring on ion time scales typically are quasineutral, i.e. have $|n_i - n_e| << n_i$. If the electrons and ions in the discharge are represented by simulation macroparticles, any attempt to calculate ϕ directly from Eq. (1) would be overwhelmed by statistical noise. For example, in a million-particle 2-D simulation with a 100×100 grid, there are typically 100 electrons or ions in each cell, and therefore the statistical fluctuations in $n_i - n_e$ within a cell would be on the order of 10%,

which is four orders of magnitude larger than the actual value. Numerical schemes involving Poisson's equation are obviously very difficult (and actually inappropriate) in the quasineutral limit. Indeed, Chen[18] noted long ago that, "In a plasma, it is usually possible to assume $n_e = n_i$ and $\nabla \cdot \mathbf{E} \neq 0$ at the same time. This is a fundamental trait of plasmas, one which is difficult for the novice to understand. *Do not use Poisson's equation to obtain E unless it is unavoidable!"*

Over the years, this approach has been followed in many analytic and numerical models which represent the plasma as a fluid, or represent the electrons as a fluid within some hybrid scheme.[19] These methods circumvent the use of Poisson's equation by neglecting electron inertia and determining E from the resulting simplified electron momentum conservation equation. In these models, n_i is determined from dynamical equations, but n_e is simply set equal to n_i to maintain quasineutrality. This procedure eliminates temporal scales on the order of the electron plasma frequency, as well as spatial structures on the Debye length scale. However, in kinetic models, and in particular in PIC simulations, the usual approach has been to calculate ϕ from Poisson's equation.

We have developed a new fully kinetic approach to the analysis and simulation of bounded, weakly collisional plasma discharges in which the bulk plasma is quasineutral. Our approach is motivated by the quasineutral fluid techniques described in the previous paragraph. At the present stage, the model specifically treats axisymmetric situations in which the electrons are strongly magnetized, as in ECR plasmas, but we believe the general approach can also be extended to three dimensions and used for unmagnetized or weakly magnetized cases, and is equally applicable to quasineutral processes in high-temperature collisionless plasma. Non-uniform externally specified magnetic fields are included, and electrostatic fields are computed self-consistently, but Poisson's equation is not used. In the numerical implementation, both electrons and ions are represented as PIC particles, with Monte Carlo collisions. The spatial gridding relects the macroscopic scale lengths, and the time steps are chosen to resolve particle motion over macroscopic lengths. We shall also give some examples in which the model provides a natural framework for analytic calculations, leading to new insights. The model has the following characteristics:

(i) Electrons are treated as guiding center particles, and in fact are firmly attached to a single flux surface. This eliminates the electron gyro time scale from the dynamics. However, the ion gyro motion is resolved both spatially and temporally, and ions are pushed through their orbits under the influence of the electrostatic and Lorentz forces (as well as collisions).

(ii) The electric field component $E_{\|}$, parallel to the magnetic field lines, is determined by the requirement that $E_{\|}$ drive the electrons to maintain quasineutrality. This field can be specified by a slightly modified form of the electron parallel momentum conservation equation with neglect of electron inertia.

(iii) Sheaths, at either grounded or floating surfaces, are regarded as thin potential barriers to electron flow. The sheath structure is not resolved, but the sheath potentials are determined self-consistently by the requirement that electron flow to walls be consistent with preservation of quasineutrality in the plasma, and also with constraints on current flow to the walls.

(iv) The Bohm condition on ion flow at the bulk-sheath interface is imposed as a boundary condition on the bulk flow. This is a key aspect of the model, since the Bohm condition is the principal constraint driving plasma flow to the walls. The quasineutral pre-sheath is resolved within the model.

(v) The relative plasma potential on different magnetic field lines, and therefore the electric field component $E_{\perp}$ transverse to the magnetic field, is determined through conditions on the transverse ion flow necessary to maintain quasineutrality. The transverse electric field and the transverse ion flow depend significantly on whether the field lines terminate on insulating or conducting walls. In the case of conducting walls, the sheath potentials and the transverse electric field are intimately related and must be determined self-consistently. In this paper, we present the formalism for both cases, and show simulation results for the insulating case, which is considerably simpler to implement.

Resonant heating of the plasma by the microwaves can also be represented in a linearized formulation which integrates analytically over the microwave and electron gyro frequencies. However, this aspect is not discussed in the present paper.

Within this framework, plasma oscillations are excluded from the model. Simulation time steps need not resolve the electron plasma or gyro frequency; thus they can be chosen to resolve motion of individual particles over macroscopic lengths of interest, and/or collisional time scales of interest. In typical cases, we use ion time steps of order few $\times 10^{-7}$ sec, and sub-cycled electron time steps of order 10^{-8} sec. The result is a very efficient code that can be run to times of real interest, e.g. milliseconds, in a few hours on a workstation. The self-consistent separation of sheath and bulk plasma also facilitates intuitive understanding and provides a useful framework for analytic calculations. For example, in Sec. 7 we shall see how self-consistent variations of the sheath potential can strongly inhibit cross-field ion transport.

2. Structure and Geometry of the Model

To help motivate the assumptions of the model, it may be useful to consider some typical plasma conditions which are of interest to us (while keeping in mind that the model is applicable to a much broader range of conditions). In ECR processing sources, the microwave frequency is usually 2.45 GHz, so that electron gyroresonance occurs at 875 G. In a two-solenoid source (Fig. 1), the magnetic field lines typically diverge downstream, so that B~1000 G where the microwaves are introduced, decreases to the resonant value nearby, and falls to as low as 20 G far downstream. The electron temperature T_e is typically a few eV. The ion temperature T_i is typically much lower, but the ion flow speed reaches the ion sound speed $c_s \equiv (T_e/m_i)^{1/2}$ at the interface between the bulk plasma and the sheath. Many gas compositions are used for processing, and pressure may vary from 0.1 mTorr to > 10 mTorr, but for specificity we shall consider Ar at pressure 1 mTorr. Typically, the plasma density will be few $\times 10^{11}$ to 10^{13} cm^{-3}, so that the ionization fraction is between 1% and 20%.

Under these conditions, the electron gyroradius is extremely small (< 1 mm) and the electron mean free path is so long (about 40 cm for electron-neutral collisions[20,21] and 30 cm for electron-ion collisions at plasma density 10^{12} cm^{-3} and $T_e = 4$ eV) that electron collisional

diffusion across field lines is very slow. Typically an electron will diffuse across field lines by < 1 cm, before eventually escaping from the system to a wall. Furthermore, we shall restrict our attention in this paper to axisymmetric systems, so that all collisionless electron drifts are azimuthal. Thus, it is quite reasonable to assume that each electron is strictly confined to a particular flux tube.[22] In the framework of r-z geometry, where the azimuthal coordinate is ignorable, we may think of the electrons as strung out along the magnetic field lines. Thus the electron motion is essentially one-dimensional in the r-z plane.

In order to treat the electron dynamics efficiently and accurately, we use magnetic field lines, denoted by a discrete index j, as one of the coordinates for our grid. The spacing of the field lines chosen for the grid is arbitrary, and in principle may be chosen to optimize the resolution in regions of particular interest. However, there are also numerical constraints on the choice of grid field lines, e.g., it is necessary to maintain an adequate number of particles on each grid field line to control statistical fluctuations. The grid used in typical simulations is shown in Fig. 2. The axial coordinate z is used as the other coordinate for the grid; equally spaced grid lines in z are denoted by the index k. The use of a non-uniform and non-orthogonal grid, which also intercepts the radial wall at oblique angles, complicates the code structure considerably, but affords great simplicity and efficiency in the treatment of electron dynamics: each electron is permanently associated with a single field line j during its entire lifetime in the system, and in the particle lay-down is linearly distributed onto the two nearest grid points, (j,k) and (j,k+1).

The ion gyroradius ranges from a few mm for thermal ions in the strong field region, to tens of cm for ions moving at c_s in the weak field region. Furthermore, the ion mean free path for charge exchange[23,24] (~ 10 cm) is often comparable to or moderately larger than the ion gyroradius. Thus the ions are only weakly magnetized. In the model, the ion orbits are computed in full 3-D, under the influence of the externally specified magnetic field, the self-consistent electric fields which are interpolated from the field line grid onto an r-z grid, and Monte Carlo collisions. After the completion of an ion time step, the ion density is laid down on the j-k grid, as follows. Each ion is attributed in z fully to its nearest neighbor grid value k, and then is apportioned among the two field lines between which it is located, according to the quadratic formula

$$\eta_{jk} = \frac{r^2_{j+1,k} - r^2}{r^2_{j+1,k} - r^2_{jk}}\ , \tag{2a}$$

$$\eta_{j+1,k} = \frac{r^2 - r^2_{jk}}{r^2_{j+1,k} - r^2_{jk}}\ , \tag{2b}$$

which is appropriate to r-z geometry. Here, the ion coordinate r is located between field lines j and j+1, with r_{jk} and $r_{j+1,k}$ the coordinates of the nearest grid points on field lines j and j+1 respectively, and η_{jk} is the fraction of the ion that is attributed to field line j.

3. Electron Dynamics and Parallel Electric Field

Since the electrons are represented as guiding center particles, each electron is characterized by its location along the field line. In the code we use the Cartesian coordinate z to specify this location, but in analytic development it is often useful to use ζ, the curvilinear coordinate along the field line. In addition, each electron has a parallel velocity $v_{||}$ and a perpendicular (gyrating) velocity $v_\perp$. We assume that the magnetic moment $\mu \equiv m_e v_\perp^2 / 2|B|$ is a constant of the motion in between collisions, so usually it is convenient to characterize the electron by its value of μ rather than $v_\perp$. The effective parallel force acting on an electron, between collisions, is then

$$F_{||} = -eE_{||} - \mu\,(dB/d\zeta), \tag{3}$$

where the second term is the mirror force. In the computational model, the electrons are pushed, between collisions, as simulation particles subject to the force $F_{||}$. The time step Δt_e for the electron push is chosen to resolve electron motion over macroscopic lengths of interest, and also to resolve electron collisional time scales. Typically Δt_e is a small fraction of the time step Δt_i used to push ions.

Let us assume for the moment that the number of electrons on a field line j is equal to the number of ions assigned to that field line, so that the field line is globally quasineutral.

(We will later discuss how to insure that this is true.) The electron Debye length is always smaller than any scale length resolved in the model, and the electron plasma frequency is always fast compared to any time scale resolved in the model. Thus, if there were any departure from local quasineutrality, the resulting strong electric field would drive electron currents parallel to **B**, which would restore quasineutrality within a time scale of several electron plasma periods, i.e. essentially instantaneously on the time scale of the model. Thus, the macroscopic parallel electric field always takes the value necessary to keep the electron density n_e equal to the ion density n_i. To specify this electric field, we can begin with the electron momentum equation. For magnetized electrons on curved field lines, this equation takes the form

$$-eE_{\|} = \frac{|B|}{n_e}\frac{\partial}{\partial \zeta}\frac{(P_{e\|}+n_e m_e u_e^2)}{|B|} + \bar{\mu}\frac{\partial |B|}{\partial \zeta} + \nu_e m_e u_{e\|} + \frac{1}{n_e}\frac{\partial}{\partial t}(n_e m_e u_{e\|}) . \quad (4)$$

Here, m_e is the electron mass, $P_{e\|} \equiv n_e T_{e\|}$ is the electron parallel pressure,

$$P_{e\|} \equiv \int dv_{\|}\, m_e (v_{\|}-u_{e\|})^2 f_e(v_{\|},v_{\perp}), \quad (5)$$

$u_{e\|}$ is the mean electron fluid velocity, $\bar{\mu}$ is the average magnetic moment at the specified location, and ν_e is the mean electron momentum transfer collision frequency.

Within the particle simulation, the first three terms on the right hand side (RHS) of Eq. (4) can be evaluated at each point of the grid, by laying down the mean quantities for the electrons assigned to that grid point. These terms represent the "ambipolar" electric field $-eE_{\|}^{(0)}$ necessary to sustain the quasineutrality relation

$$n_e = n_i \quad (6)$$

if n_i were a specified time-independent function of ζ. The remaining term (the inertial term) is a small correction, of order m_e/m_i, where m_i is the ion mass. In quasineutral fluid formulations, where n_e is simply set equal to n_i, the inertial term is neglected. However this is unsatisfactory in a particle simulation, where n_e and n_i are separately determined by the

particle evolution: if the inertial term is neglected, n_e and n_i will drift apart as n_i slowly changes and n_e does not respond. Even worse, in a particle code both n_e and n_i are subject to continual fluctuations, and the ambipolar field allows n_e and n_i to separate through these fluctuations.

There are several possible approaches to the calculation of the inertial term, or of some approximate form that couples n_e to n_i. In a previous publication,[25] we developed an approximate method in which the electrons are pushed in the ambipolar field, and then at the end of the time step a correction field is applied that is chosen to restore quasineutrality. Although this method worked well in most respects, we have found another approach that is even simpler, and very accurately conserves energy over long time scales. We simply drop the inertial term in (4) and substitute n_i for n_e in the first term of (4), so that

$$-eE_{\parallel} = \frac{|B|}{n_i}\frac{\partial}{\partial \zeta}\frac{[n_i(T_{e\parallel}+m_e u_{e\parallel}^2]}{|B|} + \bar{\mu}\frac{\partial |B|}{\partial \zeta} + \nu_e m_e u_{e\parallel}. \qquad (7)$$

Equation (7) keeps the electron density closely coupled to the ion density, while avoiding the very high-frequency plasma oscillations that are linked to the last term of (4). This can be seen by substituting (7) for $E_{\parallel}$ in the exact momentum equation (4), to obtain

$$m_e\frac{\partial u_e}{\partial t} = \left(T_e+mu_{e\parallel}^2\right)\frac{\partial}{\partial z}\ln\left(\frac{n_i}{n_e}\right). \qquad (8)$$

Equation (8) shows that the electrons are always accelerated up the gradient in n_i/n_e, i.e. toward the point of maximum positive net charge density, thereby restoring quasineutrality. We showed in Ref. 26 that this scheme is stable, preserves $n_e = n_i$ while supporting only lower-frequency oscillations, conserves energy to good accuracy, and accurately represents kinetic effects. For example, the usual dispersion relation for ion sound waves, including the Landau damping terms, can be derived.[26] We also gave several examples of successful implementation of the scheme in a one-dimensional particle simulation with no boundaries, including linear and nonlinear ion sound waves, and free expansion of a plasma.[26]

4. Sheaths at Passive Surfaces

At any material surface in contact with the plasma, there is a sheath where quasineutrality fails. We shall consider here only sheaths at unpowered or weakly dc-biased surfaces, e.g. vessel walls. The sheath thickness is typically a few times the Debye length λ_D, which is very thin for conditions of interest. For example, $\lambda_D = 15\ \mu m$ at $T_e = 4\ eV$, $n = 10^{12}\ cm^{-3}$. Such a sheath can be treated as simply a thin potential jump ϕ_s, which accelerates positive ions toward the wall, but reflects most electrons back into the plasma. At any given time, only a few electrons with high enough parallel energy can surmount the sheath potential barrier and reach the wall. (However, any electron can eventually diffuse up to high energy, due to ECR heating or electron-electron collisions, and escape from the system.) The effect of the sheath on the plasma, or on the surface, is essentially completely characterized by the sheath potential.

To determine the value of the sheath potential, we use an elaboration of the "logical sheath" scheme of Parker, Procassini and Birdsall.[27] Our formulation incorporates the Bohm flow criterion, applies appropriately to both conducting and insulating walls, and can be used for a multi-dimensional plasma with magnetized electrons. The basic idea is that the sheath potential takes the value which allows the "correct" electron flux to reach the wall. The conditions for determining the correct flux depend on whether the wall is conducting or insulating.

A. Insulating walls

An insulating wall exposed to a plasma acquires a surface charge during an initial transient period (which we do not resolve), and thereafter the electrical current density to any point on the wall must be zero. Thus the sheath potential ϕ_s at each end of field line j must take the value (the floating potential) which sets the flux of electrons, through the sheath to the wall, equal to the ion flux into the sheath from the plasma. (All positive ions which reach the boundary of the simulation pass through the sheath and reach the wall.) Furthermore, according to the Bohm criterion,[28] ions must flow from the bulk plasma into the sheath at a mean velocity equal to the ion sound speed c_s, i.e. the ion flux to any wall is

$$J_i^{Bohm} = nc_s. \tag{9}$$

In the next section we shall discuss the way in which the Bohm criterion is imposed as a boundary condition on the ion flow in the model. However, the implication for the electrons is that the electron flux to any wall, J_e^{out}, must satisfy

$$J_e^{out} = \sin\theta \int_{v_s}^{\infty} dv_{||} v_{||} f_e(v_{||}) = J_i^{Bohm}, \tag{10}$$

where

$$v_s \equiv (2e\phi_s/m_e)^{1/2}, \tag{11}$$

and θ is the angle between the magnetic field and the wall. If the electron velocity distribution function $f_e(v_{||})$ at the end of field line j is known, Eqs. (10) and (11) determine the sheath potential ϕ_s.

To implement this prescription numerically, we first push both the electrons and ions through a complete ion time step Δt_i. If an electron reaches a wall, it is reflected back along its field line, on the tentative assumption that its energy was insufficient to penetrate the sheath potential barrier. However, it is noted that that particular electron belongs to the set S_{ej}^{bounce} of electrons on field line j that reflected off the wall during Δt_i. In general, this number of electrons will be much larger than the number of ions that reach that wall during the time step, $\Delta N_{ij}^{Bohm} \equiv J_i^{Bohm} \Delta t_i A_j$, where A_j is the area intercepted on the wall by the flux tube associated with field line j. We then identify the subset S_{ej}^{out} of S_{ej}^{bounce}, consisting of the ΔN_{ij}^{Bohm} electrons which had the highest parallel energy at the moment of reflection. These electrons are assumed to have escaped during the time step; hence they are discarded. The sheath potential ϕ_{sj} is set equal to the lowest parallel kinetic energy of any of the electrons in the subset S_{ej}^{out}, at the time it reached the simulation boundary.

There are a number of numerical points which must be considered in actually implementing this scheme. The sheath potential depends on the high-energy tail of the

electron distribution, which always contains relatively few simulation electrons and is susceptible to noise. To minimize this, Δt_i must be large enough that a substantial absolute number of electrons are allowed to escape during the time step. However, the fraction of electrons which leave during Δt_i must be small. In a steady state situation, the departed electrons will be replaced by new electrons generated by ionizing collisions, and one must be careful not to overcount ionizing collisions involving electrons that actually escaped during Δt_i. Also, there may be electrons with high parallel velocities that bounce off both walls during the time step Δt_i, and these must be accounted for correctly.

B. Conducting walls

When the walls are conducting, there will typically be a boundary condition specifying the potential on any given segment of the wall. In the simplest case, the walls may all be regarded as grounded, but in other cases a dc bias may be applied. (We do not consider ac biases in this paper.) For conducting walls, there is a more complicated set of conditions that determines the sheath potentials. It is possible for non-zero electrical current density to flow to any given point on the wall, i.e. the electron flux to the wall need not be locally equal to the ion flux out of the plasma. Within the plasma, there may be currents flowing along a field line, and also ion currents flowing across field lines. However, quasineutrality imposes a constraint on the electron and ion fluxes: the total number of ions and electrons on any given field line must remain equal. This is the condition that determines the sheath potentials.

Let $J_{ej}^{out}(0)$ be the electron flux to the wall at the $z=0$ end of field line j, and $J_{ej}^{out}(z_{max})$ be the flux to the wall at the other end of field line j. Let $J_{ij}^{Bohm}(0)$ and $J_{ij}^{Bohm}(z_{max})$ be the Bohm flux of ions into the sheaths at $z=0$ and z_{max} respectively. Then maintenance of global quasineutrality on field line j requires that

$$J_{ej}^{out}(0) + J_{ej}^{out}(z_{max}) = J_{ij}^{Bohm}(0) + J_{ij}^{Bohm}(z_{max}) + \int_0^{z_{max}} dz\, \nabla \cdot J_{i\perp j}(z) . \qquad (12)$$

The last term in Eq. (12) represents the net decrease in the number of ions attributed to field line j, due to ion flow across field lines within the plasma.

In Eq. (12), the electron fluxes to the walls are determined by the sheath potentials $\phi_{sj}(0)$ and $\phi_{sj}(z_{max})$,

$$J_{ej}^{out}(z=0) = \sin\theta_{j0} \int_{-\infty}^{-v_{sj}(z=0)} dv_{||} v_{||} f_e(z=0, v_{||}), \tag{13a}$$

$$J_{ej}^{out}(z_{max}) = \sin\theta_{j,max} \int_{v_{sj}(z_{max})}^{\infty} dv_{||} v_{||} f_e(z_{max}, v_{||}), \tag{13b}$$

where

$$v_{sj}(z=0) \equiv [2e\phi_{sj}(z=0)/m_e]^{1/2},$$
$$v_{sj}(z_{max}) \equiv [2e\phi_{sj}(z_{max})/m_e]^{1/2}, \tag{13c}$$

θ_{j0} is the angle between field line j and the wall at $z=0$, and $\theta_{j,max}$ the angle at $z=z_{max}$. If the walls are grounded (ϕ=0), then the plasma potential just inside the sheath, at either $z=0$ or z_{max}, is just equal to the sheath potential. However, the difference between the plasma potentials $\phi_j(z_{max})$and $\phi_j(0)$ is given by the line integral of $E_{||}(z)$, the parallel electric field given by Eq. (7). Thus the two sheath potentials are related by

$$\phi_{sj}(z_{max}) - \phi_{sj}(0) = -\int_0^{z_{max}} dz E_{||}(z), \tag{14}$$

and Eq. (12) in effect specifies *both* sheath potentials, provided the electron energy distributions and the ion flux are known from the simulation.

If there is an externally imposed potential difference along field line j, between the walls at $z=0$ and z_{max}, then Eq. (14) takes the more general form

$$\phi_{sj}(z_{max}) - \phi_{sj}(0) = \phi_{ext} - \int_0^{z_{max}} dz E_{||}(z), \qquad (15)$$

where ϕ_{ext} is the imposed potential difference. While Eq. (12) specifies the total electron flux escaping from the field line, Eq. (15), together with the rest of the simulation equations, determines separately the flux of electrons to the walls at $z = 0$ and z_{max}, and thus in effect the electric current flowing along the field line. In this way, the simulation calculates the electric current density in terms of the imposed voltage, i.e. it gives a macroscopic Ohm's law for the plasma.

It is clear from this formulation that in the case of conducting walls the sheath potentials are intimately connected to the cross-field ion flow. We shall see that it is necessary to calculate both the sheath potentials and the ion flow self-consistently at each time step. Therefore we shall defer the discussion of a scheme for actually calculating the sheath potentials to Sec. 6, where the ion dynamics are discussed.

5. Imposition of the Bohm Criterion as a Boundary Condition

In Sec. 4, we have shown how to specify the correct sheath potential, and impose this potential barrier as a boundary condition to the electron flow. In a real plasma, or in a model that calculates the internal electric field through Poisson's equation, a sheath with the correct potential will very quickly form, as a response to the rapid initial loss of electrons to the wall. Simultaneously, the ions will be accelerated to a mean speed $u_i^{\perp}$, normal to the wall, given by

$$u_i^{\perp} = c_s \qquad (16)$$

at the interface between the quasineutral bulk plasma and the ion-rich sheath. Indeed, it is well known that a steady-state monotonic sheath, with $n_i > n_e$, can form only where the ion flow in the bulk plasma satisfies Eq. (16). This is known as the Bohm criterion.[1,28]

In a magnetized plasma, an ion-rich sheath will form at every surface which the magnetic field lines intersect at an angle greater than $(m_e / m_i)^{1/2}$. As long as there is an ion-rich sheath, the Bohm criterion (16) normally holds, independently of the direction of the magnetic field; in (16), we use the notation $u_i^{\perp}$ with superscript $\perp$ to denote the velocity normal to the wall, not to the magnetic field.

However, our quasineutral model, as described in the preceding sections, describes only the bulk plasma and simply assumes the existence of a sheath, without requiring that the appropriate bulk flow conditions obtain. Equation (16) is not a consequence of the quasineutral model; steady state solutions exist which satisfy Eq. (16), but there are also solutions which exhibit other ion flow patterns at the walls. For example, if the ions are initially cold and uniform and the electrons are isothermal throughout the bulk plasma, the electron pressure will remain uniform, no electric field will be generated, and there will be no ion flow toward the wall. Thus, within our model, the Bohm condition must be imposed externally as a boundary condition to the ion flow, which is necessary to specify the correct solution of the equations. One may say, from the perspective of the bulk plasma, that the Bohm condition *causes* the flow of the plasma toward the walls.

Within the context of a fluid model of the quasineutral bulk plasma, Eq. (16) can be imposed as a boundary condition to the ion momentum equation. But how is one to impose Eq. (16) as a boundary condition within a particle simulation? We have used a procedure that seems to imitate the dynamical process that sustains the Bohm condition within the quasineutral bulk part of a real discharge.

In a real plasma, the ion flow speed is equal to c_s at the edge of the bulk plasma, but falls off to a much lower value within the interior of the plasma. The continuity equation then implies that n_i falls off at the edge of the bulk plasma. Quasineutrality requires that $n_e = n_i \equiv n$. Assuming T_e does not vary as rapidly as n at the plasma edge, the fall-off in electron pressure at the edge leads to an ambipolar electric field [first term of Eq. (7)] which sustains the ion flow in the "presheath" region. In the model, we define a thin strip of depth d, adjacent to any material surface, with d chosen to be macroscopically small but larger than $c_s \Delta t_i$. Within the strip, we lay down the ion velocities to determine the average ion flow speed $u_{ij}^{\perp}$ normal to the surface, on field line j. We then add an increment $\delta u_{ij}^{\perp}$ to all of

the ion velocities, such as to bring $u_{ij}^{\perp}$ to c_s. This procedure insures that n_i falls off at the perimeter of the bulk plasma just as it would if Bohm flow were occurring. The resulting pressure drop at the perimeter leads (over a time scale characterized by the ratio of the presheath width to c_s) to the formation of an appropriate presheath. Bohm flow is thereafter self-sustaining, but only neutrally stable, with the increment $\delta u_{ij}^{\perp}$ a small adjustment at each time step.

The Bohm flow condition, together with the sheath potential as specified in Sec. 4, together represent a complete set of boundary conditions for the quasineutral bulk plasma. We shall refer to this as the "Bohm logical sheath" procedure.

6. Transverse Electric Field, and Ion Transport Across Magnetic Field Lines

In Sec. 3 we showed how to determine the parallel electric field $E_{\parallel}$ from the requirements of quasineutrality, as applied to the electron flow along field lines. Thus, the relative potential between any two points on the same field line is known. If the absolute potential were specified at any single reference point on each field line, say at $z = 0$, then it would be known everywhere, and the transverse electric field $E_{\perp}$ could also be computed. This additional information can also be obtained from the requirements of quasineutrality, but it is bound up with the ion flow, rather than the electron flow. The conclusions also depend fundamentally on whether the field lines end on insulating walls or on grounded conducting walls.

A. Insulating walls

In the case of insulating walls, electrical current cannot flow from the plasma to any point on the walls. Furthermore, in our model no transverse electron current is permitted within the plasma. It follows that if there is non-zero net ion flux onto any field line within the plasma, a violation of quasineutrality will occur on that field line. In a real plasma, a large potential would immediately build up all along the field line, leading to a reversal of

the net transverse ion flow onto the field line, and subsequently to a train of ion plasma oscillations. To model this as an effect within a quasineutral framework, we shall stipulate that the integrated net ion flux onto any field line is zero, i.e.

$$\int dz \nabla_\perp \cdot (n\mathbf{u}_i) = 0. \tag{17}$$

Equation (17) is well satisfied on time scales longer than the ion plasma frequency, expresses the condition of quasineutrality, and can be used to solve for the reference potential, $\phi(z=0)$, on each field line.

To implement Eq. (17) numerically, we begin with the known electric field at the previous time step t^m, assume that quasineutrality was satisfied at t^m, and that the flux condition (17) was satisfied at the previous half-time step $t^{m-1/2}$. First, we push each ion to a new velocity $\mathbf{v}^*$ at time $t^{m+1/2}$, using the electric fields determined at t^m, and to a new position (r^*,z^*) at time t^{m+1}. At the end of the time step, there may be a small inequality of order Δt_i^2 between the number of ions N_{ij}^* and electrons N_{ej}^* on field line j, since the flux continuity condition is satisfied exactly at time $t^{m-1/2}$, but may be inaccurate by order Δt_i during the time step:

$$\Delta N_j^* \equiv N_{ij}^* - N_{ej}^* \neq 0 \quad (\text{order } \Delta t_i^2). \tag{18}$$

This is an indication that a correction potential $\delta\phi_j$ should have been added to the assumed potential on field line j, so as to maintain the flux continuity equation (17) throughout the time step. This may be thought of as the correction to the reference potential $\phi_j(z=0)$. The corresponding correction to the radial electric field is

$$\delta E_{r,jk} = (\delta\phi_j - \delta\phi_{j+1}) / (r_{j+1,k} - r_{jk}) \tag{19}$$

at z-grid point k, between field lines j and j+1. This in turn leads to a correction velocity

$$\delta v_{r,jk} = (e\delta E_{r,jk} / m_i)\, \Delta t_i \tag{20}$$

and a position displacement

$$\delta r_{jk} = (e\delta E_{r,jk} / m_i)\,\Delta t_i^2 \tag{21}$$

for every ion in this grid cell. Using Eqs. (19) - (21), the resulting correction to the number of ions on field line j can then be written as

$$\delta N_{i\perp j} = a_{j-1}\delta\phi_{j-1} - (a_j + a_{j-1})\delta\phi_j + a_j\delta\phi_{j+1}, \tag{22}$$

where the coefficients a_j are determined by first summing up the displacements of the particles, enumerated with the index n, which are attributed to z-grid point k and lie between field lines j and (j+1), and then summing up the contributions of each grid point k to the total number of ions on field line j. Given that the ions are apportioned among adjacent field lines according to the quadratic scheme (2), the coefficients are found to be[29]

$$a_j = \frac{e\Delta t_i^{\,2}}{m_i}\sum_k \frac{1}{(r_{j+1,k}^2 - r_{jk}^2)\,(r_{j+1,k} - r_{jk})} \sum_n \left[2r_n + \left(\frac{dr^2}{dz}\right)\left(\frac{dr}{dz}\right)\right]. \tag{23}$$

The quantity $\delta N_{i\perp j}$ from Eq. (22) is then set equal to $-\Delta N_j^*$, so that the quasineutrality condition becomes

$$a_{j-1}\delta\phi_{j-1} - (a_j + a_{j-1})\delta\phi_j + a_j\delta\phi_{j+1} = -\Delta N_j^*. \tag{24}$$

Equation (24) is a linear ordinary difference equation which determines $\delta\phi_j$, the correction to the potential $\phi_j(z=0)$ which is necessary to maintain global quasineutrality.[30] In this way, the potential difference between field lines is specified. After $\delta\phi_j$ has been calculated, the ions are pushed again in the corrected fields. Each field line j will then have $N_{ij} = N_{ej}$ at time t^{m+1}, and Eq. (17) will be satisfied at $t^{m+1/2}$.

It will be noted that this procedure determines the plasma potentials and the ion flow in a coupled self-consistent way. However, the sheath potentials and the electron flow play

no role in this determination. As we shall see, the situation is different when the walls of the vessel are conducting; in this case, the sheath potentials and the escape of electrons to the walls must also be included self-consistently in the calculation.

B. Grounded walls

In the case of grounded walls, the wall serves as a zero point for the potential that is common to all field lines. The potential in the bulk plasma on field line j, just inside the sheath at $z=0$, is thus equal to the sheath potential ϕ_{sj}. If ϕ_{sj} is known, the potential can be calculated at any point on the field line, and the transverse E-field can then be calculated by taking differences of potentials on adjacent field lines. However, the sheath potential is determined from Eqs. (12) - (14), which involve the ion transverse flow. Thus the transverse ion flow is coupled to the escape of electrons through the sheaths.

To numerically implement the solution to this coupled problem, let us begin by rewriting Eq. (12) in the discrete form

$$\Delta N_{ej}^{out} = \Delta N_{ij}^{Bohm} - \Delta N_{i\perp j}, \tag{25}$$

Here ΔN_{ej}^{out} is the total number of electrons on field line j that escape to the walls, through the sheaths at both ends, during time Δt_i. For any given electron energy distribution, ΔN_{ej}^{out} is a strong nonlinear function of ϕ_{sj}. ΔN_{ij}^{Bohm} is the total number of ions that escape to the walls from flux tube j during time Δt_i. $\Delta N_{i\perp j}$ is the net change in the number of ions attributed to field line j, due to transverse ion flow within the plasma.

The numerical solution of Eq. (25) is similar in spirit to the approach used for the case of insulating walls, but much more complicated in practice. Let us assume that the plasma was quasineutral at the previous time step t^m, that the sheath potentials ϕ_{sj}^m are known at t^m, and that Eq. (25) was satisfied at that time. We can then push the ions to new velocities v^* at $t^{m+1/2}$ and positions (r^*,z^*) at t^{m+1}, using the potentials known at time t^m. From the new ion positions, we can calculate a provisional value of $\Delta N_{i\perp j}$, which we shall call $\Delta N_{i\perp j}^*$. ΔN_{ij}^{Bohm} is slowly varying and can be evaluated at the beginning of the time step. However, in

general Eq. (25) will not be exactly satisfied at the end of the new time step (again the error will be of order Δt_i^2), because the ion and electron distributions in phase space will have changed a little since the previous time step, and the flux condition (12) will have been in error by order Δt_i.

This is indicative that an increment $\delta\phi_{sj}$ should have been added to the sheath potentials ϕ_{sj}, so as to preserve the flux condition throughout the time step and the quasineutrality condition at the end of the time step. In accordance with the reasoning that led to Eq. (22), this leads to a correction $\delta N_{i\perp j}$ to $\Delta N_{i\perp j}$, given by

$$\delta N_{i\perp j} = a_{j-1}\delta\phi_{s,j-1} - (a_j + a_{j-1})\delta\phi_{sj} + a_j\delta\phi_{s,j+1}, \tag{26}$$

where the coefficients a_j are again given by Eq. (23). Now Eq. (25) can be written as

$$a_{j-1}\delta\phi_{s,j-1} - (a_j + a_{j-1})\delta\phi_{sj} + a_j\delta\phi_{s,j+1} + \Delta N_{ej}^{out}(\phi_{sj}^m + \delta\phi_{sj}) = \Delta N_{ij}^{Bohm} - \Delta N_{i\perp j}^*. \tag{27}$$

The RHS of Eq. (27) can be regarded as known, so Eq. (27) is an ordinary difference equation that determines the increments to the sheath potential $\delta\phi_{sj}$. The equation is strongly nonlinear through the term ΔN_{ej}^{out}. Once the $\delta\phi_{sj}$ are known, the ions are pushed again in the newly determined potentials, and the electrons with energy exceeding the sheath potential are allowed to escape to the wall, as discussed in Sec. 4. Thus the computation can proceed, with the ion dynamics, the sheath potentials, and the transverse electric fields computed self-consistently at each time step.

The reader may have noticed that the calculation of the sheath potential correction $\delta\phi_{sj}$ is performed fully implicitly in conjunction with the particle push. This is in fact necessary for numerical stability: as will be seen in the next section, the sheath potential exerts a diffusive effect on transverse ion current, and the natural time step for this diffusion is shorter than we wish to resolve. Everything else in the computation is done explicitly.

7. Nature of ion transport

A. Insulating walls: field-aligned flow model

Section 6A makes it clear that *net* ion transport across field lines is impossible in an insulating vessel, since the plasma must remain quasineutral and electron transport across field lines is negligible. However, it is quite possible for there to be a non-zero transverse ion flux at particular locations along a field line. Any transverse flux at one location must be canceled out by a reverse flux elsewhere along the field line. Thus, in situations where there are strong variations along a field line (as in Fig. 2 where the field lines flare outward downstream) one may find patterns of cross-field ion eddy flow. In the next section we shall see an example of this type of behavior in our simulations.

Nevertheless, we shall consider here a simple solvable one-dimensional fluid approximation, in which the ion flow is assumed to be field-aligned. This model, which extends the work of Godyak and collaborators[31] to the case of flow along curved magnetic field lines, helps to interpret the two-dimensional simulations, and provides insight into the way in which the plasma temperature, density, and other properties are determined by the quasineutrality condition, the ambipolar potential, the Bohm boundary condition, and the requirement of global power balance. In the model, the electrons on any single field line are represented as an isothermal fluid. The ions are treated as a cold fluid, with field-aligned flow velocity u_i, subject to an electric field $E_{||} = -\partial\phi / \partial\zeta$ and a constant mean free path λ_i for (predominantly charge exchange[24]) collisions with stationary neutrals. In addition, we assume that electron-impact ionization proceeds at frequency ν_I, a function of T_e. In steady state, the ion continuity and momentum conservation equations, and the Boltzmann relation

$$e[\phi - \phi(\zeta=0)] = T_e \ln[n / n(\zeta=0)], \tag{28}$$

can be reduced to a single ordinary differential equation for the normalized ion flow velocity $u \equiv u_i/c_s$,

$$(1-u^2)\frac{du}{ds} - \frac{u^2|u|}{\lambda} - u\frac{d\ln B}{ds} = \nu \tag{29}$$

and a quadrature for the normalized density,

$$\frac{n(s)}{n(0)} = \exp\left[-\int_0^s ds'\, u\left(\frac{|u|}{\lambda} + \frac{du}{ds'}\right)\right]. \tag{30}$$

In Eqs. (29) and (30), $s \equiv \zeta/\zeta_{max}$, $\nu \equiv \zeta_{max}\nu_I/c_s$, and $\lambda \equiv \lambda_i/\zeta_{max}$, where ζ is the curvilinear coodinate along the field line and $\zeta = 0$, $\zeta = \zeta_{max}$ are the points at which the field line intersects the vessel walls.

The boundary conditions for Eq. (29) arise from the Bohm condition, but some discussion is needed as to the proper way to apply the Bohm condition within a model of 1-D ion flow along field lines. If the field line intersects the walls normally, the appropriate boundary conditions on the field-aligned velocity u_i are given directly by the Bohm condition as stated in Eqs. (16),

$$u_i(0) = -c_s, \tag{31a}$$

$$u_i(\zeta_{max}) = +c_s. \tag{31b}$$

But if the field line intersects the walls obliquely, at angles θ_0 and θ_{max} at $\zeta = 0$ and ζ_{max}, the appropriate boundary conditions at the sheath edge are Eqs. (16) for the velocity component normal to the wall. To the extent that flow within the quasineutral plasma is strictly field-aligned, this would then give

$$u_i(0) = -c_s/\sin\theta_0, \tag{32a}$$

$$u_i(\zeta_{max}) = +c_s/\sin\theta_{max}. \tag{32b}$$

However, Eqs. (32) are clearly not acceptable boundary conditions, since Eq. (29) becomes singular when $|u| = 1$. The resolution to this dilemma is that one-dimensional flow along field lines is not a consistent model, even within the quasineutral plasma, at a point where the field lines intersect a wall obliquely. There is always a pre-sheath structure,[32] beginning

about where Eqs. (31) are satisfied, wherein the ions are accelerated toward the wall and the density falls off by a factor of order $\sin\theta$. Thus the consistent boundary conditions, within the region where one can use a model of field-aligned ion flow, are indeed Eqs. (31).

The *two* boundary conditions (31) applied to the single first-order ordinary differential equation (29) are an indication that Eqs. (29) and (31) together constitute a nonlinear eigenvalue problem: the ionization coefficient ν_I must take the value necessary to permit a solution. Since ν_I is a rapidly increasing function of T_e, Eqs. (29) and (31) actually determine the discharge temperature, as well as the velocity profile $u_i(\xi)$. The normalized density profile $n(\xi)/n(0)$ and the normalized potential $[\phi(\xi)-\phi(0)]/T_e$ are then determined by Eqs. (30) and (28). The *absolute* plasma density is determined by the power balance

$$W_{in} = W_{out} = \left[n(0)c_sA_\perp(0)+n(\xi_{max})c_sA_\perp(\xi_{max})\right]\left[\epsilon_I+e\phi_s+\frac{5}{2}T_e\right], \quad (33)$$

where W_{in} is the microwave power input to the flux tube, W_{out} is the energy loss rate due to electrons and ions reaching the walls, and $A_\perp(\xi)$ is the cross-sectional area of the flux tube at ξ. For Maxwellian electrons and cold ions, the energy loss per escaped ion is the sum of ϵ_I, the electron inelastic collison energy loss per ionization (including excitation, dissociation, etc. as well as ionization); $e\phi_s+T_e/2$, the ion energy at the wall; and $2T_e$, the mean thermal energy of an escaping electron.

Equations (28)-(31) show that the normalized profiles $u_i(\xi)/c_s$, $n(\xi)/n(0)$ and $[\phi(\xi)-\phi(0)]/T_e$ depend only on the collisionality parameter λ and the *shape* of the magnetic field lines (but not the magnitude of the magnetic field). The temperature T_e is determined by the requirement that the ionization rate be just sufficient to replace the ions lost to the walls. Since the eigenvalue ν is $\xi_{max}\nu_I/c_s$, the ionization rate ν_I is inversely dependent on the field line length ξ_{max}. In more physical terms, ions escape more rapidly from shorter field lines, and thus the ionization rate (i.e. T_e) must be larger to replace the lost ions. The density must be lower on these field lines so that a specified level of microwave power, divided among fewer electrons, is sufficient to raise T_e to the required value.

In Fig. 3, we show a solution of Eqs. (28)-(31) for a case with $\lambda = 0.27$, $\xi_{max} = 35$ cm, and

$$B = B_0 \exp\left[-\frac{\zeta^2}{(26.9\ \mathrm{cm})^2}\right], \tag{34}$$

corresponding roughly to one of the long interior field lines of Fig. 2, with the gas being argon at pressure 1 mTorr. A strong left-right asymmetry is evident, introduced by the non-uniform magnetic field. At $z = 0$, the ions are accelerated in a standard presheath of thickness $\sim\lambda_i$, but to the right the ions are accelerated by an electrostatic force arising from the mirror effect, and the plasma density falls off as the field lines diverge. Thus there is less need on the right for presheath acceleration to satisfy the Bohm condition, and indeed the presheath is less evident.

In Fig. 4, we show how the electron temperature T_e on a particular field line depends on ζ_{max}, the length of that field line, with $B(\zeta)$ given by (34). Referring to the geometry shown in Fig. 2, we note that ζ_{max} is essentially the same for all the interior field lines that terminate on the end wall, but decreases steadily as we go to the outer field lines that terminate on the radial wall. Thus the 1-D model predicts that T_e will be constant on the interior field lines, but will steadily increase on the outer field lines. Similarly, the average density $<n>$ on a particular field line is predicted to be constant on the interior lines but steadily decreasing on the outer field lines that terminate on the radial wall. The 1-D model of Eqs. (28) - (31), (33) has no dependence on the angles θ_0 and θ_{max}, so there is no discontinuity in plasma properties between the last field line that terminates (nearly normally) on the end wall and the first that terminates (at glancing incidence) on the radial wall. As we shall see in Sec. 8, this is not a realistic representation of the 2-D flow. In the 2-D simulation, field lines which intersect the radial wall lose ions much more rapidly, and thus T_e is larger and the average density $<n>$ is smaller for field lines that terminate on the radial wall.

We note that the rate at which ions escape from a field line is proportional to the ratio of the density at the walls to the mean density on the field line, $\eta \equiv [n_j(0)+n_j(\zeta_{max})]/2<n_j>$. For this reason, T_e and $<n_j>$ are sensitive to the density profile $n_j(\zeta)/n_j(0)$ along the field line. Within our 1-D model, η is determined by the solution of Eqs. (29) - (31), but in our 2-D simulations other effects enter to change the density profile, and thereby also the mean values T_{ej} and $<n_j>$.

B. Cross-field transport in grounded conducting vessels

In the case of grounded conducting walls, Simon[34-36] showed in 1955 that ions can diffuse across magnetic field lines at a rate characterized by the ion gyroradius and mean free path, without dragging the electrons across field lines. Quasineutrality is maintained by electron flow to the walls along field lines. These calculations have been refined over the years,[35] and in the present context of weakly magnetized ions, and strong electric fields required to satisfy the Bohm condition, correspond to mobility-limited or inertially limited transverse ion flow.[36] However, the effect of the spatial variation of the sheath potential, induced by the ion flow, has traditionally been omitted from these models. Our quasineutral formulation of the sheath-coupled transverse flow lends itself to an exploration of this effect, which turns out to be dominant in the case of internal perturbations. The sheath potential strongly inhibits non-uniformities in the divergence of the transverse ion flow, as can be seen from the following considerations. Suppose that momentarily the flow is such as to increase the number of ions on field line j, more rapidly than the number of ions on adjacent field lines. To maintain global quasineutrality on field line j, it is necessary to reduce the electron flow to the walls from field line j, in accordance with Eq. (25). Therefore, the sheath potential on field line j increases. But this also increases the plasma potential everywhere along field line j, and thus opposes the net ion transverse flow onto the field line. To gain analytic insight into this effect, we shall consider some very simplified model problems chosen to elucidate particular aspects of the problem.

Linearized fluid treatment

Consider a plasma contained within grounded walls at $z = 0$ and $z = L$, but unbounded in the x and y directions. Let the magnetic field $\mathbf{B}_z$ be uniform and along the z-direction. Since we wish to focus on the effect of sheath potentials, which are normally very large compared to potential variations within the bulk plasma, we shall assume the bulk plasma in equilibrium is uniform with density n_o, plasma potential ϕ_o (equal to the sheath potential),

and temperatures T_e and T_i. However, we recognize the existence of a presheath at the walls by allowing the density at the walls, n_w, to be smaller than n_o by a factor η. We then consider a small deviation from equilibrium, with perturbations n(x), $\phi(x)$ and $u_x(x)$ to the density, sheath potential and ion flow velocity, each of the form e^{ikx}. Assume for convenience that the perturbation maintains the isothermal character of the plasma, and also the ratio η of wall to bulk density.

We begin with the linearized ion momentum equation, which takes the form

$$n_o \frac{\partial u_x}{\partial t} + \frac{ikP_i}{m_i} + \frac{en_o}{m_i} ik\phi + \nu_i' n_o u_x = 0, \tag{35}$$

where

$$\nu_i' \equiv \nu_i \left\{ 1 + \frac{\Omega_i^2}{\nu_i^2} \right\}, \tag{36}$$

ν_i is the ion-neutral momentum transfer collision frequency, and the second term in (36) results from the magnetization of the ions, i.e. from the $v_y \times B_z$ force. (This form is appropriate when $\partial u_y/\partial t << \nu_i$.)

We can relate ϕ to n by linearizing Eq. (12). Defining a normalized distribution $F_e(v_z)$ by $f_e(v_z) = (n_o+n)F_e(v_z)$, the pertubation to the total electron flux to the two walls is

$$J_e^{out} = 2\eta n \int_{(2e\phi_o/m_e)^{1/2}}^{\infty} dv_z v_z F_e(v_z) - \frac{2\eta n_o}{m_e} F_e\left(\left(\frac{2e\phi_o}{m_e} \right)^{1/2} \right) e\phi. \tag{37}$$

The perturbation to the ion flux to the two walls is

$$J_i^{Bohm} = 2\eta n c_s,$$

while the effect of the transverse ion flow is contained in the last term of Eq. (12), $\int_0^L dz \nabla \cdot J_{i\perp} = ikLn_o u_x$. Substituting these quantities in Eq. (12), we find

$$e\phi = -\frac{ikLm_e}{2\eta F_e(e\phi_o)} u_x. \tag{38}$$

For the case of a Maxwellian distribution, where equilibrium requires

$$\frac{e\phi_o}{T_e} = \frac{1}{2}\ln\left(\frac{m_i}{2\pi m_e}\right), \tag{39}$$

Eq. (39) reduces to

$$e\phi = -(ikL/2\eta)\,(m_iT_e)^{1/2}u_x. \tag{40}$$

To complete the calculation, we use the isothermal relation $P_i = nT_i$ and the perturbed ion continuity equation,

$$\frac{\partial n}{\partial t} + ikn_o u_x + \frac{\eta n c_s}{L} - \nu_I n = 0, \tag{41}$$

where ν_I is the ionization rate. The last two terms of (41) cancel, since in equilibrium $\eta n_o c_s = \nu_I n_o L$. Using (40) and (41) in (35), we arrive at an equation for u_x,

$$\frac{\partial^2 u_x}{\partial t^2} + \frac{k^2 T_i}{m_i} u_x + \frac{k^2 L c_s}{2\eta}\frac{\partial u_x}{\partial t} + \nu_i \frac{\partial u_x}{\partial t} = 0. \tag{42}$$

Each of the last three terms of Eq. (42) leads to a distinct type of response. The first term, in combination with the second term, leads to sound waves among the ions. These are ordinary sound waves associated with the ion pressure and propagating at the ion *thermal* speed, not the ion sound speed. The last term of Eq. (42) represents ordinary collisional damping. The third term of (42), which arises from the response of the sheath potential, is the most interesting term. Taken together with the first term, the third term leads to diffusion of u_x, i.e. it is formally similar to a bulk viscosity term. The sheath potential thus leads to a dissipative effect which drives the flow toward uniformity of the velocity gradient $\partial u_x/\partial x$. In typical situations, this is the dominant term. To demonstrate this formally, consider the normal modes of Eq. (42),

$$u_x(x,t) = u_x(0)\, e^{ikx+pt}, \tag{43}$$

where

$$p = -\left(\frac{k^2 L c_s}{4\eta} + \frac{\nu_i'}{2}\right) \pm \left[\left(\frac{k^2 L c_s}{4\eta} + \frac{\nu_i'}{2}\right)^2 - \frac{k^2 T_i}{m_i}\right]^{1/2}. \tag{44}$$

The modes are always damped, and if

$$\frac{kL}{\eta}\left(\frac{T_e}{T_i}\right)^{1/2} + \frac{2\nu_i'}{k}\left(\frac{m_i}{T_i}\right)^{1/2} > 4. \tag{45}$$

they are purely damped with no oscillation. Since $T_e/T_i >> 1$, inequality (45) will normally be satisfied. For short wavelength modes, the dissipative effect arising from the electron sheath potential response easily dominates over the effect of ion pressure, and quickly drives the system back to uniformity in transverse velocity.

In a simulation code, the time scale for this diffusive process, $\tau_{dif} = 2\eta/k^2 L c_s$, can be very short. In typical applications of our code, we may have $L \simeq 35$ cm, $c_s \simeq 3\times10^5$ cm/s, $\eta \simeq 0.3$, and the shortest wavelength modes have π/k equal to the spacing of the field lines used in the grid, as small as 0.3 cm. This gives $\tau_{dif} = 5\times10^{-10}$. Since we wish to use time steps much longer than this, it is necessary to calculate the sheath potential implicitly, as discussed in Sec. 6.

Nonuniform microwave heating

It is important to note that the dissipative effect discussed in the preceding paragraph drives the system toward uniform transverse flux, not toward uniform density. This distinction has important consequences. Consider, for example, the "high mode" of an ECR discharge,[37] in which all of the injected microwave energy is absorbed. The power density deposited into plasma heating thus depends only on the microwave flux, not on the plasma density or other details of the plasma state. The rate of creation of new electron-ion pairs by

electron-impact ionization is then simply proportional to the microwave flux. Now suppose there is a small sinusoidal perturbation to the microwave flux, which leads to an ionization rate of the specified form $\dot{n}_{I0} + \dot{n}_I e^{ikx}$. Then the plasma density will have a similar perturbed form, $n_o + ne^{ikx}$. If there were no ion transport across field lines, the density perturbation would simply be proportional to the ionization source perturbation,

$$\frac{n}{n_0} = \frac{\dot{n}_I}{\dot{n}_{I0}}. \tag{46a}$$

If, on the other hand, the ions can freely diffuse or flow across field lines, the non-uniformity in density will be smoothed out, i.e.

$$\frac{n}{n_0} \to 0. \tag{46b}$$

To determine n/n_0 correctly, we use Eqs. (35), (40), and the linearized continuity equation,

$$\frac{\partial n}{\partial t} + ikn_o u_x + \frac{\eta n c_s}{L} - \dot{n}_I = 0. \tag{47}$$

[Note the difference in the last term on the LHS of (47), as compared to Eq. (41) where the ionization source is assumed to be isothermal.] Neglecting the effect of ion collisions, the steady state solution of Eqs. (35), (40), and (47) is given by[38]

$$\frac{n}{n_0} = \frac{\dot{n}_I}{\dot{n}_{I0}} \frac{T_e}{T_e+2T_i}. \tag{48}$$

Comparing with Eq. (46a), we see that transverse ion transport does reduce the density perturbation, but only by a factor $T_e/(T_e+2T_i)$ which is very close to unity. Diffusion toward uniformity in density is strongly *inhibited* by the sheath potential response.

Ion transport to vessel walls

We have seen that the response of the sheath potential strongly suppresses *internal* cross-field flows within the plasma. However, it has been known for decades[34] that loss of ions to the walls, through non-ambipolar cross-field flow, is an important process in conducting vessels. The sheath potential response can influence this flow, but it does not change the general conclusion. The effect of the sheath potential is merely to induce a smooth flow pattern which has uniform divergence, i.e. reduces the density at a comparable rate on different field lines.

A more systematic discussion of cross-field transport, for discharges within conducting vessels, will be provided in future publications.

8. Simulation of an ECR discharge in an insulating vessel

An axisymmetric simulation code **QUASI-rz** has been developed which implements the formalism presented in Secs. 1 - 6. Electrons are represented as particles transported along the field lines, as discussed in Sec. 3. Each electron is characterized by its position z, its parallel velocity, and the value of its magnetic moment (which is equivalent to knowing the magnitude of its perpendicular velocity). Ions are represented as particles characterized by position in the r-z plane and by all three components of velocity, as discussed in Sec. 6. Within the plasma, parallel electric fields are calculated as in Sec. 3, and transverse fields as in Sec. 6. Sheaths at passive surfaces are represented as thin potential barriers, as in Sec. 4, while the Bohm boundary condition is imposed as in Sec. 5. Electron-neutral and ion-neutral collisions are included, via a Monte Carlo step (using the null-collision method[39,40]) which occurs at the end of each particle push step. Electron-electron collisions are included in the Monte Carlo step via the recently-developed Langevin formulation of multiple small-angle scattering,[41] which is a great advance in efficiency over previous numerical formulations in terms of binary collisions.

The code is ultimately intended to provide a complete kinetic picture of an ECR discharge. We shall present here a sample calculation, which somewhat oversimplifies the

representation of ECR experiments which are ongoing at NRL,[42-48] but nonetheless illustrates a number of interesting points. The geometry is taken to be a cylindrical insulating vessel of length 35 cm and radius 7 cm, representing the source region of the ECR, as illustrated in Fig. 2. The magnetic field configuration, as shown in Fig. 2, is the actual field applied in the experiment, ranging from 1 kG at $z=0$ to 171 G at $z=35$ cm. The gas is argon at pressure 1 mTorr, and a collision set is used which includes accurate cross sections for electron-neutral[49] and ion-neutral elastic scattering,[50] electron-impact ionization and excitation,[49] and ion-neutral charge exchange.[50,51] Leonhardt, et al[47] have recently shown that interactions between metastables and other components are not important in high-density Ar plasma at these pressures, so these are not included in the collision set.

The representation of electron cyclotron heating is simplified in the present simulation. We do not calculate the propagation of the microwaves or the details of their interaction with the electrons. Rather, we heat the electrons by giving each electron a random kick in transverse velocity every time it crosses the resonant surface, which lies in the plane $z=4$ cm. The magnitude of the kick $\Delta v_\perp$ is chosen randomly from a Maxwellian distribution $(2\pi)^{-1/2}\exp[-(\Delta v_\perp)^2/2\Delta^2]$. The root-mean-square value Δ is chosen so that the total power absorbed by all the electrons on field line j is equal to $P_\mu(r_{j,res})A_{j,res}$, where $P_\mu(r)$ is the specified microwave power density, $r_{j,res}$ is the value of r where field line j intersects the resonant surface, and $A_{j,res}$ is the area of flux tube j on the resonant surface. In the present simulation, we use

$$P_\mu(r) = P_o \exp(-r^2/r_o^2), \tag{49}$$

with $P_o = 1.8$ W/cm^2 and $r_o = 7$ cm. The total absorbed microwave power, integrated from $r=0$ to the wall at $r=7$ cm, is then 350 W.

Given the simplication of the geometry and of the ECR heating process, one cannot necessarily expect the simulation to provide a quantitatively acccurate picture of any particular experiment. However, the model includes all of the important effects that determine the plasma properties, including spatial variation of parameters, flow patterns, velocity distribution functions, and ionization fractions.

Simulation results

We chose (arbitrarily) to initiate the simulation with uniform temperature $T_e = 6.6$ eV and plasma density n(r,z) proportional to B(z,r), with $n = 1.5\times10^{12}$ at $z = 0$. After a time of order 300 μs the simulation evolves to a steady state, which appears to be insensitive to the initial conditions. We shall show graphics illustrating the steady state plasma at time 500 μs.

Figure 5 shows the plasma density n(r,z). The peak density is 6.3×10^{12} cm^{-3}, in reasonable agreement with experimental results. Curiously, the peak is seen to be off-axis, with a 20% density dip on axis, even though the microwave power is gently peaked on-axis. As we shall see, this is a consequence of two-dimensional flows which differ from the field-aligned flow model of Sec. 7A.

Figure 6 shows surface plots of the ion fluid velocity components $i_{iz}(r,z)$ and $u_{ir}(r,z)$. We note that ions flow to all walls at flow velocity $u_i^{\perp} \simeq c_s$, in accordance with the Bohm condition. At every wall, a presheath is evident in Figs. 5 and 6, wherein the ions are accelerated to c_s, but the presheath is minimal on the downstream end wall where the acceleration largely occurs as a consequence of magnetic field expansion. Figure 7 is a vector plot of the ion flux, which more clearly illustrates the surprisingly complex nature of the flow. The important feature is that the outer field lines of Fig. 2, which intersect the radial wall at an acute angle of 5° to 19°, lose ions to the wall over a relatively large area at perpendicular velocity $u_i^{\perp} = c_s$. This loss of ions is not resupplied through flow along the field line, as in the model of Sec. 7A, but mainly through cross-field flow from adjacent field lines. However, the quasineutrality condition specifies that no field line can have a net gain or loss of ions through cross-field flow within the plasma. Thus, there must be an inward return flow upstream. Comparing Fig. 7 with Fig. 2, it can be seen that the result is a flow pattern which is fairly close to field aligned, and yet shows a significant cross-field eddy flow structure.

The nature of the flow has a significant impact on the density and temperature profile within the plasma. The cross-field flow permits the rate of ion loss from those field lines

that terminate obliquely on the radial wall to be greater than the loss rate from the interior field lines that terminate nearly normally on the end wall. (Recall that in the 1-D model of Sec. 7A, the loss rate depends only on the length of the field line, but not on the angle at which the field line intersects the wall.) Thus there is an abrupt decrease in the plasma density, as we move from the last field line that terminates on the end wall ($j = 9$) to the first field line that terminates on the radial wall. This is evident in Fig. 5. In Fig. 8 we plot the average value of the density $< n_j >$ on field line j, as a function of j. This figure shows even more clearly the sharp change in the plasma around field line $j = 9$. As j increases further, i.e. as we consider the outer field lines that terminate at decreasing values of z, ions are lost still faster and there are further decreases in $< n_j >$.

The electron temperature T_e, which is found to be quite close to isotropic, is shown as a surface plot in Fig. 9. T_e is close to flat, as expected, on the inner field lines $j \leq 9$. On field lines $j > 9$, which terminate on the radial wall, T_e increases as the field line becomes shorter. This is a consequence of the more rapid loss of ions on these short field lines, as discussed in Sec. 7A. However, the electron temperature, which we define as the mean $< 3m_e v^2/2 >$, is found to be significantly larger than the values obtained from the fluid model of Sec. 7A. The primary reason for this is that the electron energy distribution function falls off from Maxwellian in the high energy regime, which controls electron-impact ionization. Thus T_e must be somewhat larger to give the appropriate ionization rate. Distribution functions will be discussed in more detail in forthcoming work. This temperature and density pattern is seen in the NRL experiments.[46]

The cross-field ion flow also leads to a rather subtle effect on the density of the interior field lines. At large z (downstream), the flow is divergent and depletes the ions, but in the region of highest density near $z = 10$ cm, the flow is convergent and brings in additional ions. Thus this flow tends to increase the peakedness of the density profile $n_j(z)$ along a field line, i.e. to increase the maximum of n_j but reduce n_j at the ends of the field line. Figure 7 shows that the cross-field eddy flow is strongest on the field lines (j=7,8,9) that terminate at the outside of the end wall. On field lines that are near the axis, the flow is very nearly field-aligned. Thus the density profile $n_j(z)$ is more peaked on field lines j=7,8,9 than on the inner field lines near the axis. However, the loss rate of ions to the walls

is proportional to the density at the end of the field line, and thus is slower on field lines j=7,8,9. Applying the arguments of Sec. 7A in this more general multidimensional context, reducing the particle loss rate increases the density all along the field line. This is the explanation of the off-axis density peak which can be seen in Fig. 5 at $z = 8$, $r = 2.8$, and which is also evident in Fig. 8.

The potential profile $\phi(r,z)$, shown in Fig. 10, is more complex than might have been anticipated. It is not peaked on axis, and it is not simply indicative of the electron pressure profile, as in an unmagnetized plasma. Rather, $\phi(r,z)$ has a saddle at on axis at $z = 9$, and for $z \lesssim 15$ cm ϕ is a monotonically increasing function of r, except in the presheath at the radial wall. Downstream, ϕ is a monotonically decreasing function of r. This structure is just what is needed to drive the radially outward ion flow downstream, and the inward return flow upstream. This type of potential structure has been observed in the NRL experiments.[46]

9. Concluding Remarks

We have presented a variety of techniques for modeling the quasineutral region of a plasma discharge. These include methods for: (i) determining the electric field parallel to **B**, and the associated electron transport; (ii) determining the potential variations transverse to **B**, and the associated ion transport; (iii) determining the spatially and temporally dependent sheath potential; (iv) enforcing the Bohm flow condition. All of these techniques are time-dependent and fully kinetic, and based on PIC modeling of both the electrons and ions. In all cases, the fields and potentials are determined directly from the requirement of quasineutrality. Poisson's equation is not used, the Debye shielding length is effectively set to zero, and electron plasma oscillations are not present in the modeling. As a result, the models focus on the macroscopic processes that are actually of interest, and permit the use of large time steps and spatial gridding that enhance computational efficiency.

The modeling techniques have been discussed in the context of magnetized ECR discharges for processing applications, but we believe that they lend themselves to a wide range of plasma conditions, including unmagnetized plasmas, unbounded plasmas, and high-temperature collisionless plasmas of interest in fusion and space physics.

The power of the techniques has been demonstrated by applying them analytically to some simple fluid situations, and by incorporating them in a two-dimensional (axisymmetric) PIC simulation model for an ECR discharge. Analytic study of discharge contained within a conducting vessel revealed significant modifications to the classic Simon diffusion across a magnetic field.[34-36] Simulation of an ECR discharge contained within insulating walls revealed unanticipated and important structural features, which are dependent on 2-D ion flows.

In this paper we have not discussed the modeling of the microwave-plasma interaction. Computationally efficient approaches to this problem will be discussed in subsequent publications. Simulation of discharges within conducting vessels are also in progress and will be reported in future publications.

Acknowledgments

We especially acknowledge contributions by Richard F. Fernsler to our understanding of collisional processes and many other matters. We appreciate the stimulation provided by interactions with our experimental colleagues, including Scott Douglass, David Hinshelwood, Charles R. Eddy, Vasgen Shamamian, Darrin Leonhardt, James E. Butler, Bruce Weber, and others. We are also grateful to Irving Haber for many good ideas about numerical techniques, and to Noah Hershkowitz for sharing his insight. This work was supported by the Office of Naval Research.

References

1. M. A. Lieberman and A. J. Lichtenberg, "Principals of Plasma Discharges and Materials Processing," Wiley-Interscience, New York, 1994.
2. C. K. Birdsall, IEEE Trans. Plasma Sci. **19**, 65 (1991).
3. R. W. Boswell and I. J. Morey, Appl. Phys. Letters **52**, 21 (1988).
4. D. Vender and R. W. Boswell, IEEE Trans. Plasma Sci. **18**, 725 (1990).
5. M. Surendra, D. B. Graves, and I. J. Morey, Appl. Phys. Letters **56**, 1022 (1990).
6. R. K. Porteus and D. B. Graves, IEEE Trans. Plasma Sci. **19**, 204 (1991).
7. D. B. Graves, H. Wu, and R. K. Porteus, Japan. J. Appl. Phys. **32**, 2999 (1993).
8. V. P. Gopinath and T. A. Grotjohn, IEEE Trans. Plasma Sci. **23**, 602 (1995).
9. V. Vahedi, C. K Birdsall, M. A. Lieberman, G. DiPeso, and T. D. Rognlien, Plasma Sources Science Technol. **2**, 261 (1993).
10. M. M. Turner and M. B. Hopkins, Phys. Rev. Lett. **69**, 3511 (1992).
11. K. A. Ashtiani, J. L Shohet, W. N. G. Hitchon, G.-H. Kim, and N. Hershkowitz, J. Appl. Phys. **78**, 2270 (1995).
12. J. Denavit, J. Comput. Phys. **42**, 337 (1981).
13. R. J. Mason, J. Comput. Phys. **41**, 233 (1981).
14. A. Friedman, A. B. Langdon, and B. I. Cohen, Comments Plasma Phys. and Controlled Fusion **6**, 225 (1981).
15. A. B. Langdon, B. I. Cohen, and A. Friedman, J. Comput. Phys. **51**, 107 (1983).
16. J. U. Brackbill and B. I. Cohen, eds., "Multiple Time Scales," Academic Press, 1985, Chapters 8, 9, 11.
17. D. W. Hewett and D. J. Lawson, J. Comput. Phys. **101**, 11 (1992).
18. F. F. Chen, "Introduction to Plasma Physics," Plenum Press, New York, 1974, p. 66.
19. R. J. Mason, in Ref. 16, Chapter 8.
20. L. S. Frost and A. V. Phelps, Phys. Rev. **136**, 1538 (1964).
21. L. G. Christophorou, "Atomic and Molecular Radiation Physics," Wiley-Interscience, New York, 1970.
22. Since azimuthal drift velocities play no role in any of the considerations of this paper, we shall consistently use the notation $v_\perp$ to refer to the electron gyration speed, not including any drift. If it is necessary to calculate azimuthal electron drifts, this can be done within the framework of the model. Also, it is possible to include electron cross-field transport as a slow collisional diffusion, but this will not be discussed further in this paper.
23. A. V. Phelps, J. Chem. Phys. Reference Data **20**, 557 (1991).
24. See Ref. 1, p. 78. The cross-section for elastic ion-neutral scattering is comparable to the charge exchange cross-section, but elastic scattering is predominantly at very small angles. In this connection, see M. L. Vestal, C. R. Blakley, and J. H. Futrell, Phys. Rev. A **17**, 1337 (1978).

25. M. Lampe, G. Joyce, and W. M. Manheimer, to be published in *Lectures in Plasma Physics and Technology*, edited by V. Stefan, La Jolla International School of Physics, 1997.
26. G. Joyce, M. Lampe, and W. M. Manheimer, NRL Memorandum Report 6794-97-7893; J. Comp. Phys. (1997), to be published.
27. S. E. Parker, R. J. Procassini, and C. K. Birdsall, J. Comput. Phys. **104**, 41 (1993).
28. K.-U. Riemann, J. Phys. D: Appl. Phys. **24**, 493 (1991). See also Ref. 1, p. 158.
29. When the magnetic field lines are oblique, the correction potentials $\delta\phi_j$ also lead to a perturbation to v_z, which makes an additional contribution to $\delta N_{i\perp j}$; this appears as the last term of Eq. (23).
30. For the case in which the discharge is contained wholly within insulating walls, there is no way to specify the plasma potential with respect to the outside world. The ion flow depends only on the relative potential between adjacent field lines, and thus the quasineutrality condition should specify all but one of the potentials ϕ_j. Indeed, it can be seen that Eqs. (22) are redundant, and can be solved for all but one of the potentials.
31. V. A. Godyak, *Soviet Radio Frequency Discharge Research*, Delphic Associates, Falls Church, VA, 1986. See also Ref. 1, p. 137.
32. For example, in the case of a plasma with well-magnetized ions, it is known that there is a pre-sheath structure, on the scale length of the ion Larmor radius, where the ion flow cannot be treated as field-aligned. See G.-H. Kim, N. Hershkowitz, D. A. Diebold, and M.-H. Cho, Phys. Plasmas **2**, 3222 (1995).
33. See Ref. 1, pp 80-81.
34. A. Simon, Phys. Rev. **98**, 317 (1955).
35. A. Simon, "An Introduction to Thermonuclear Research," Pergamon, New York, 1959.
36. See Ref. 1, pp. 140-145.
37. D. A. Carl, M. C. Williamson, M. A. Lieberman, and A. J. Lichtenberg, J. Vac. Sci. Tech. **B9**, 339 (1991), and earlier references contained therein.
38. The derivation of Eq. (40) assumed T_e uniform, but this isothermal relation cannot hold exactly in the present circumstances. However, it is still permissable to use (40): the perturbations to T_e are typically much smaller than those to n, because the ionization rate responds exponentially to T_e but only linearly to n.
39. J. P. Boeuf and E. Marode, J. Phys. D **15**, 2169 (1982);
40. S. L. Lin and J. N. Bardsley, J. Chem. Phys. **66**, 435 (1977).
41. W. M. Manheimer, M. Lampe, and G. Joyce, NRL Memorandum Report 6709-97-7894; J. Comp. Phys., in press. Electron-ion collisions are also easily treated using the formulation in Manheimer, et al, but they are not included in the simulation shown in Sec. 8 of this paper.
42. S. R. Douglass, C. R. Eddy, Jr., and B. V. Weber, IEEE Trans. Plasma Sci. **24**, 16 (1996).
43. G. Mehlman, C. R. Eddy, Jr., and S. R. Douglass, J. Appl. Phys. **78**, 6421 (1995).

44. S. R. Douglass, C. R. Eddy, Jr., and B. V. Weber, submitted to IEEE Trans. Plasma Sci. (1966).
45. C. R. Eddy, Jr., O. J. Glembocki, D. Leonhardt, V. A. Shamamian, R. T. Holm, B. D. Thoms, J. E. Butler, and S. W. Pang, J. Electronic Materials, in press (1997).
46. C. R. Eddy, Jr., D. Leonhardt, S. R. Douglass, B. D. Thoms, V. A. Shamamian, and J. E. Butler, submitted to J. Vac. Sci. Tech. A (1997).
47. D. Leonhardt, C. R. Eddy, Jr., V. A. Shamamian, R. F. Fernsler, and J. E. Butler, submitted to J. Appl. Phys. (1997).
48. D. Leonhardt, C. R. Eddy, Jr., V. A Shamamian, R. T. Holm, O. J. Glembocki, B. D. Thoms, J. E. Butler, and S. W. Pang, submitted to Appl. Phys. Lett. (1997).
49. K. Tachibana, Phys. Rev. A **34**, 1007 (1986).
50. A. V. Phelps, J. Chem. Ref. Data **20**, 557 (1992).
51. M. L. Vestal, C. R. Blakley, and J. H. Futrell, Phys. Rev. A **17**, 1337 (1978).

Table 1. TYPICAL PARAMETERS FOR AN ECR REACTOR

Microwave frequency	$f_o \sim 2.45 \times 10^9$ Hz
Pressure	P ~ 0.5 - 10 mTorr
Magnetic field	$B_o \sim 20$ - 1000 Gauss
Plasma density	$n_e \sim n_i \sim 10^{11}$ - $10^{13}/cm^3$
Electron temperature	$T_e \sim$ 1-10 eV

Nominal Time Scales

Electron plasma oscillation	10^{-11} sec
Electron gyration	6×10^{-11} sec
Electron transit through ECR zone	10^{-8} sec
Electron collision frequency	10^{-7} sec
Ion plasma period	10^{-7} sec
Ion gyration	10^{-5} sec
Ion collision frequency	10^{-5} sec
Ion lifetime	10^{-4} sec
Neutral residence time	10^{-2} sec

Spatial Scales

Debye length	< 0.01 cm
Electron gyroradius	0.005 to 0.2 cm
Sheath thickness	0.1 cm
Electron mfp	few to 10's of cm
Microwave wavelength	< 12 cm
Ion gyroradius	up to few cm
Ion mfp	mm's to cm's
Device size	10 - 100 cm

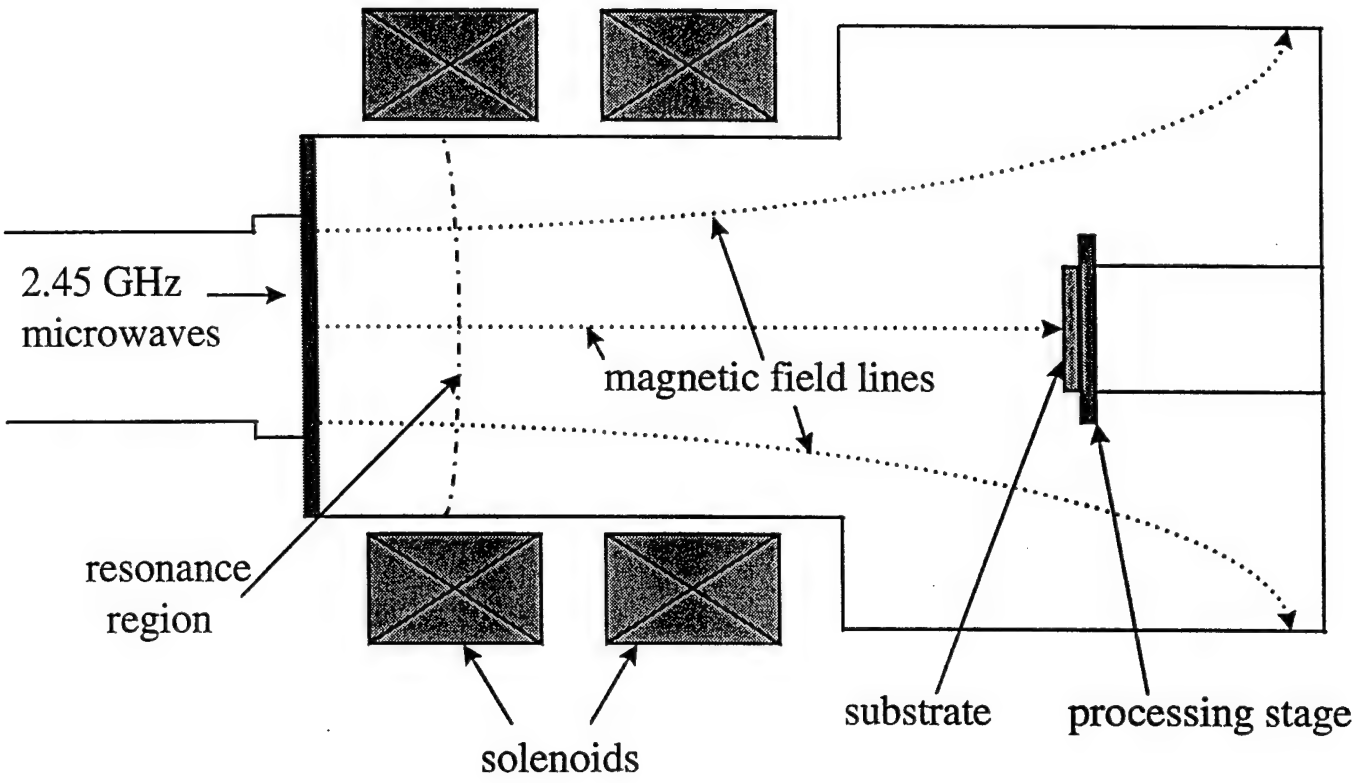

Fig. 1 — Schematic drawing of a typical two-magnet ECR plasma reactor.

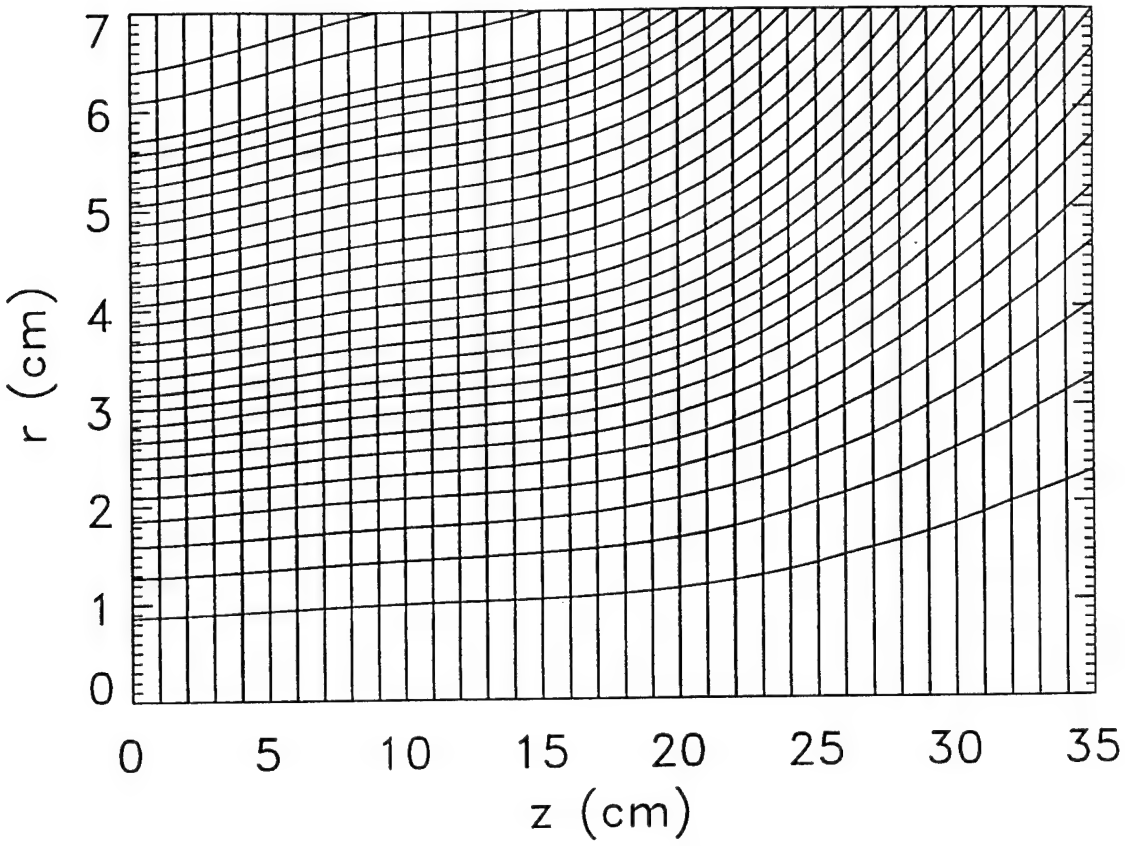

Fig. 2 — In the simulation shown in this paper, the geometry of the ECR source is simplified to a cylinder. The simulation grid, shown in this figure, is formed by a chosen set of magnetic field lines (the actual measured field lines in an experimental configuration), and by an equally spaced z-grid.

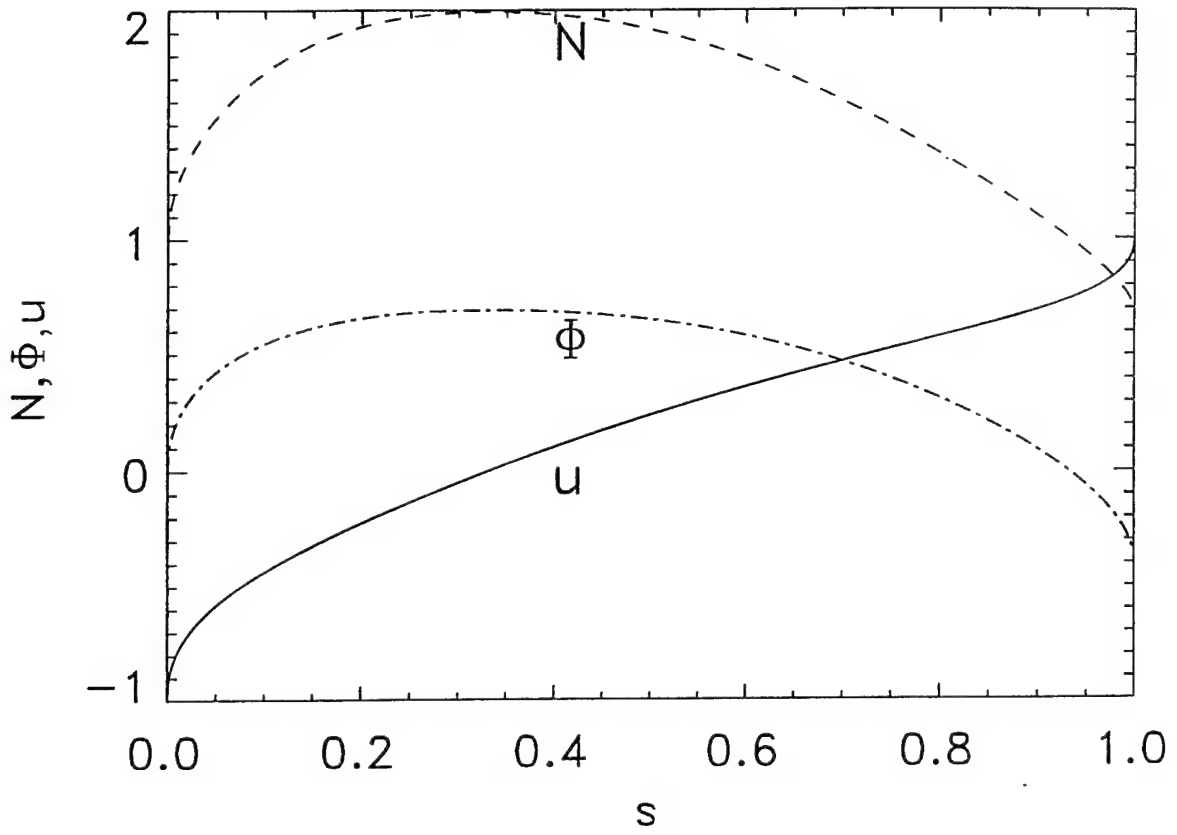

Fig. 3 — Plasma state obtained by solution of the 1-D field-aligned flow model, Eqs. (28) - (31), for conditions approximating the long field lines of Fig. 2. Shown are the normalized density $N(s) \equiv n(s)/n(0)$ (dashed curve), the normalized ion flow velocity $u(s) \equiv u_i(s)/c_s$ (solid curve), and the normalized plasma potential $\Phi(s) \equiv [\phi(s)-\phi(0)]/T_e$ (dot-dashed curve). The eigenvalue is $\nu = 1.56$, corresponding to $T_e = 3.4$eV.

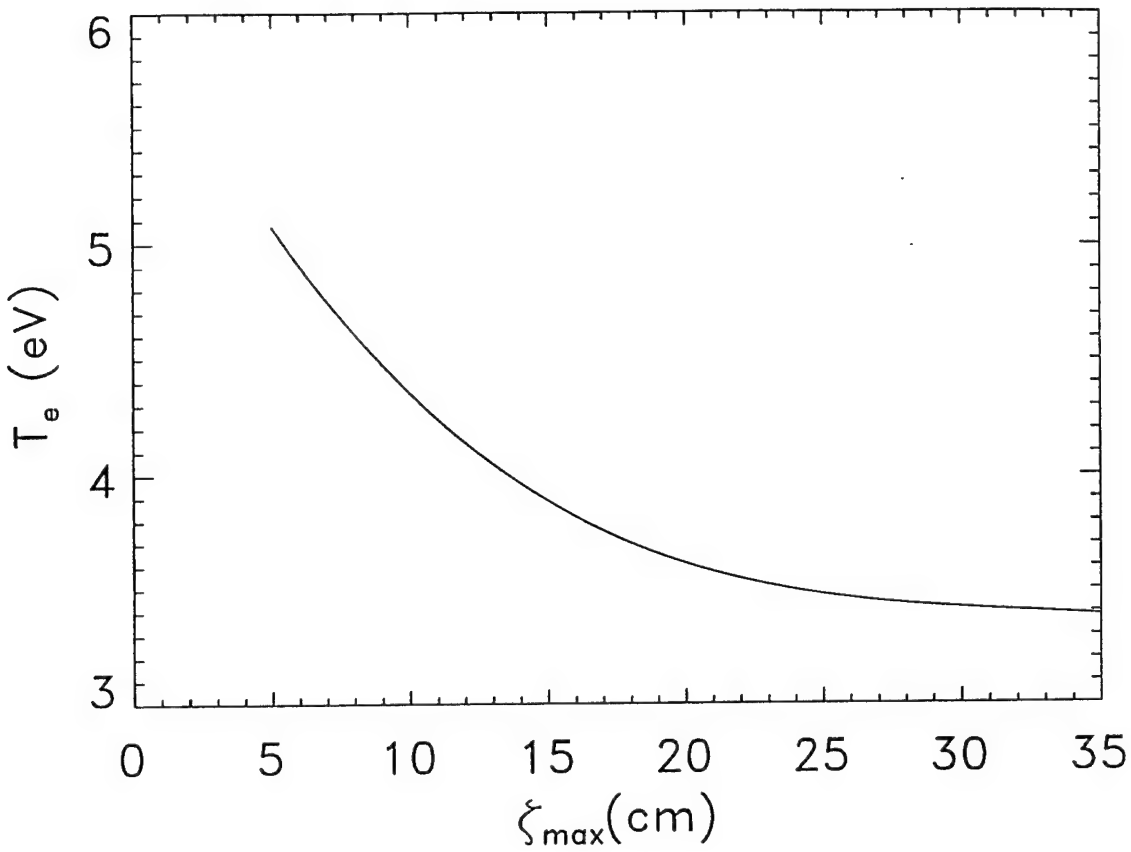

Fig. 4 — T_e as a function of field line length ζ_{max}, from the 1-D field-aligned flow model of Sec. 7A, for conditions approximating the magnetic field configuration of Fig. 2.

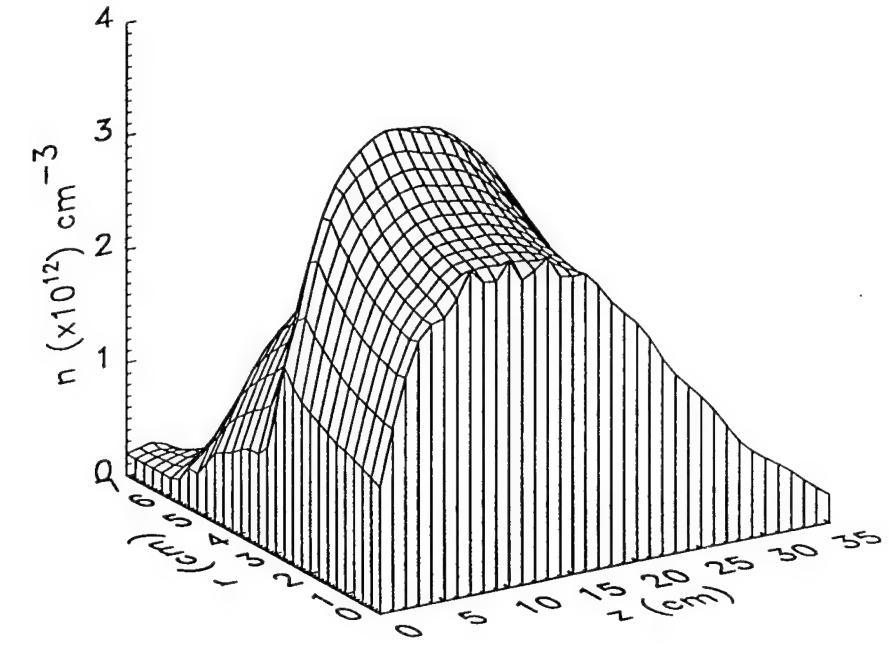

(a)

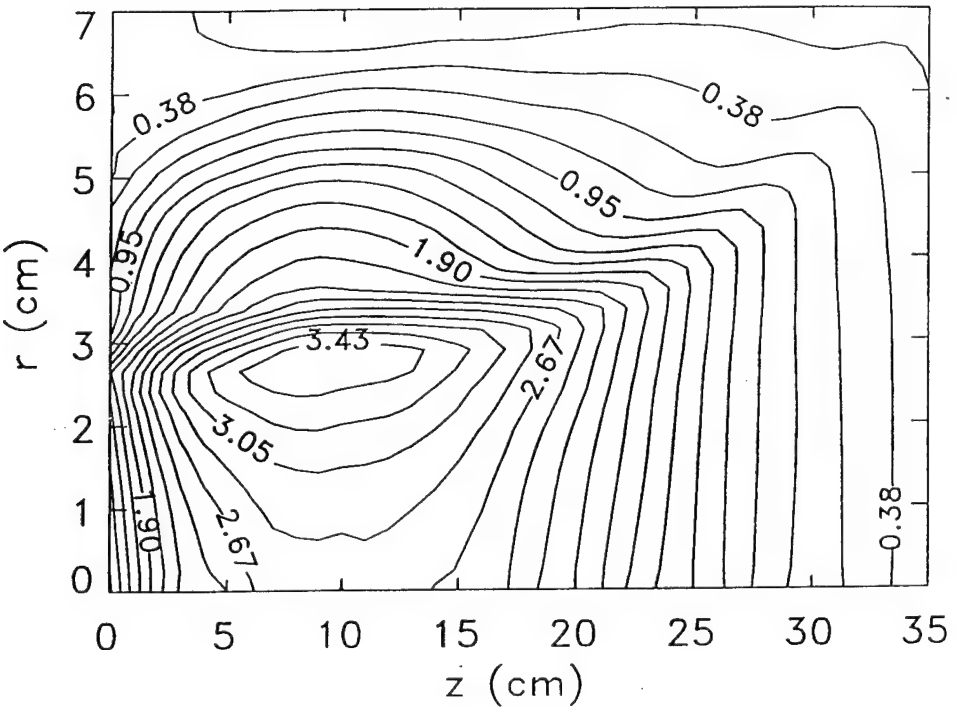

(b)

Fig. 5 — Plasma density n(z,r)×10^{12} cm^{-13}, shown as a surface plot (a) and a contour plot (b), at time 500 μs, taken from a **QUASI-rz** simulation with Ar pressure 1 mT, microwave power 350 W, and insulating vessel walls.

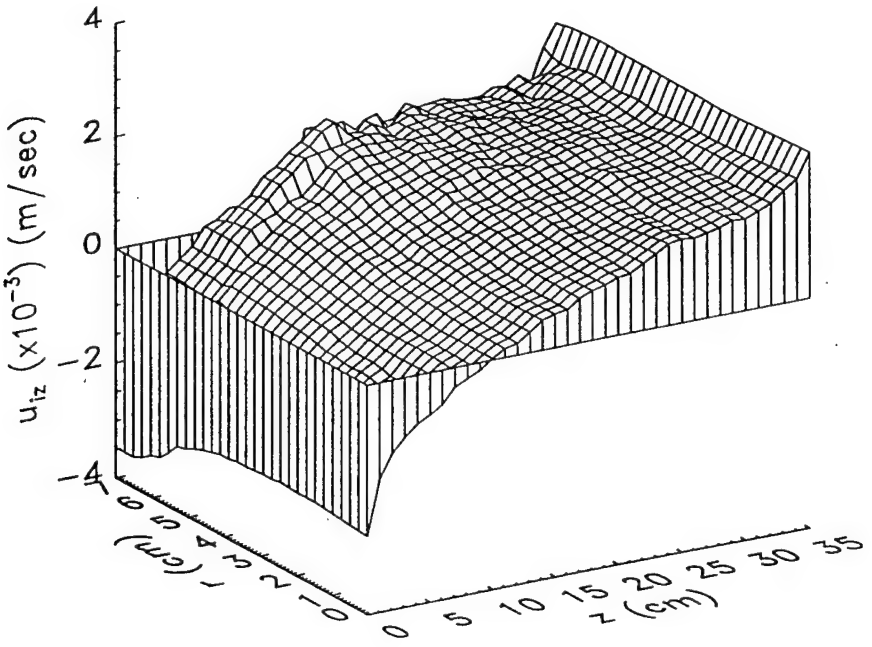

(a)

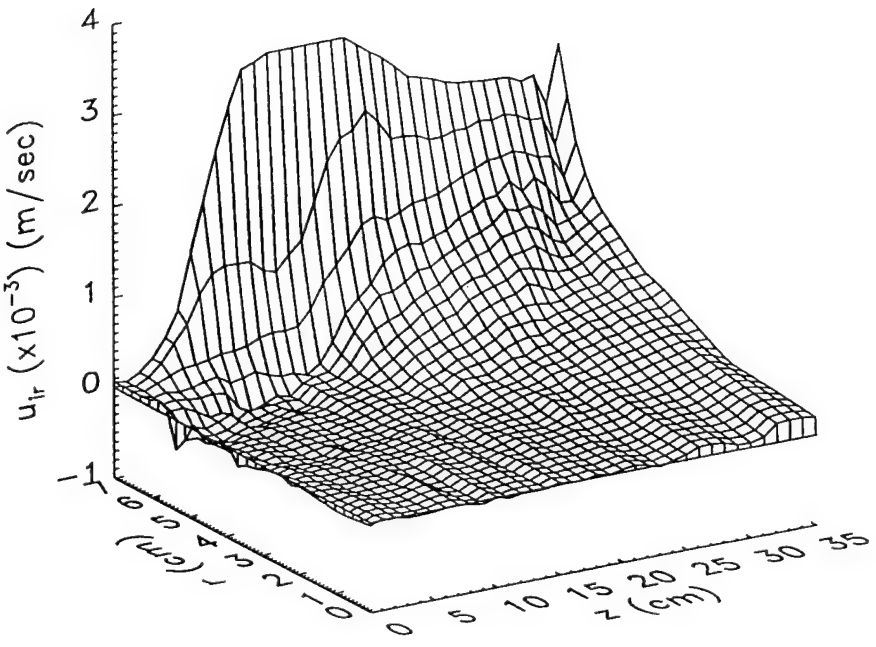

(b)

Fig. 6 — Surface plot of the ion fluid velocity components (a) u_{iz} and (b) u_{ir} at time 500 μs, from the simulation of Fig. 5.

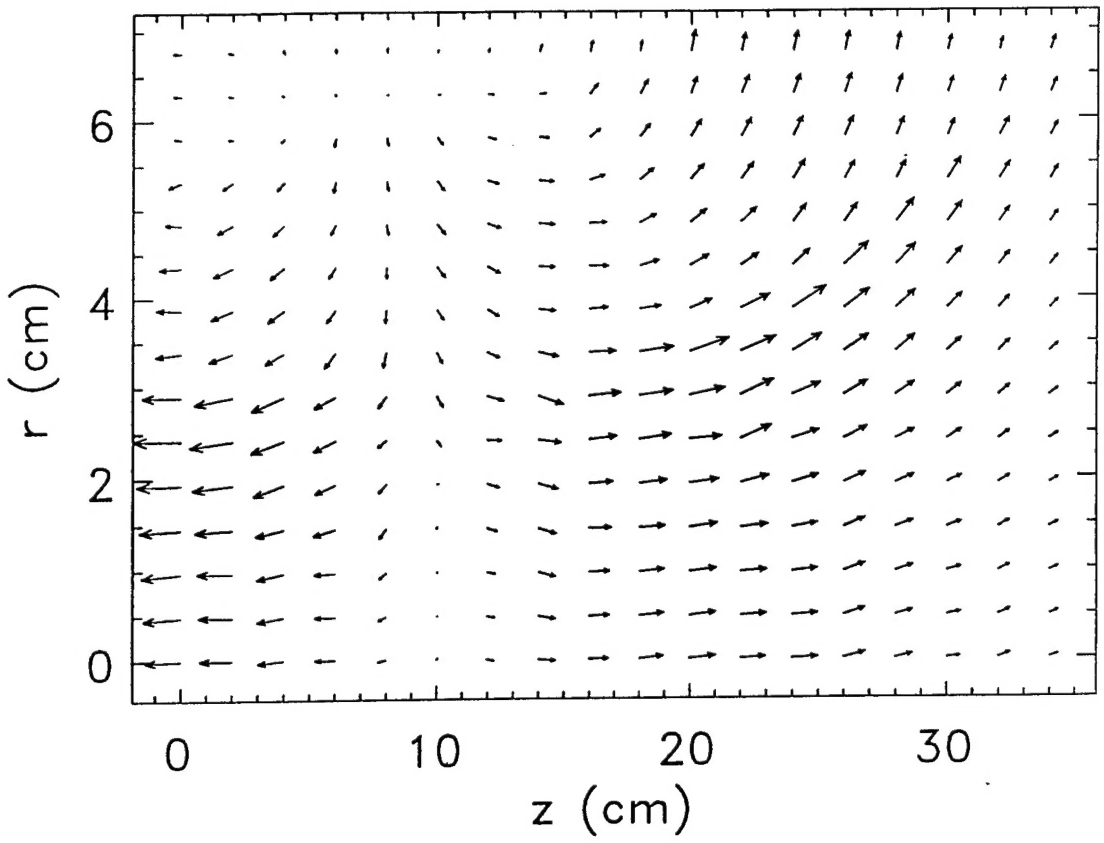

Fig. 7 — Vector plot of the ion flux at time 500 μsec, from the simulation of Fig. 5. Note that the aspect ratio of the plot is different from that of the simulation.

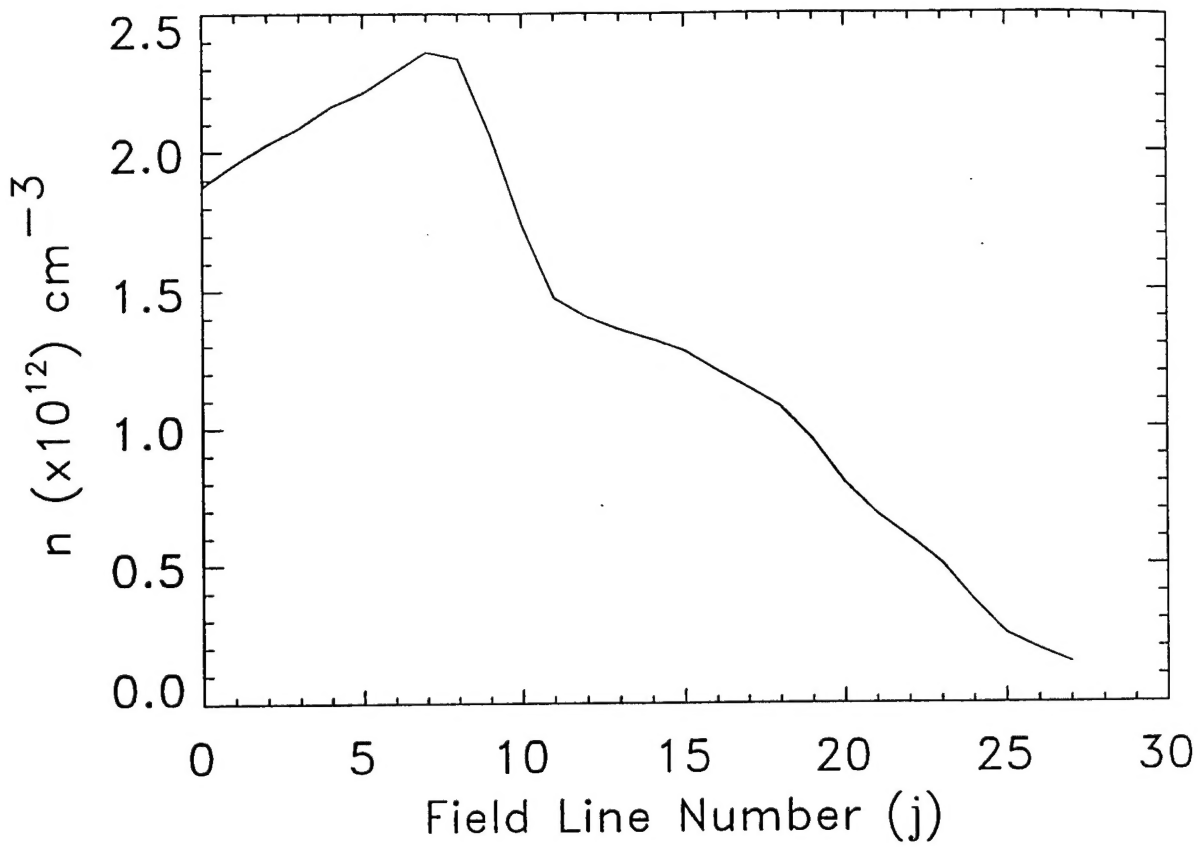

Fig. 8 — The average density on field line j at time 500 μsec, as a function of the field line number.

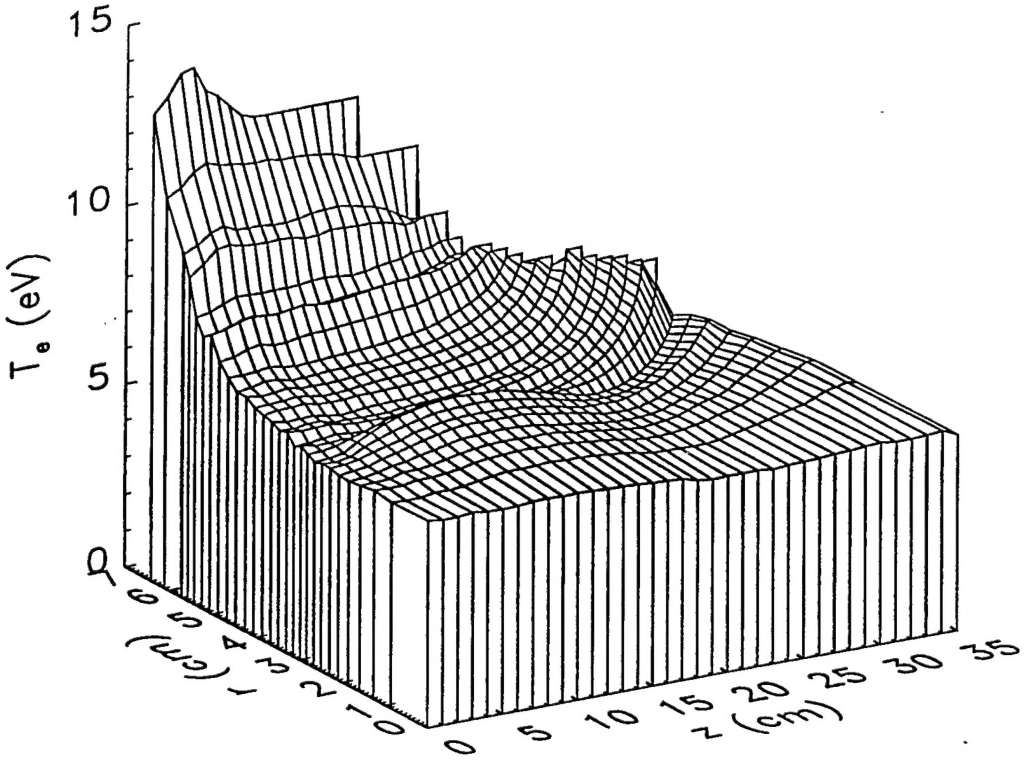

Fig. 9 — Surface plot of electron temperature T_e, defined as $<2m_e v^2/3>$, at time 500 μsec.

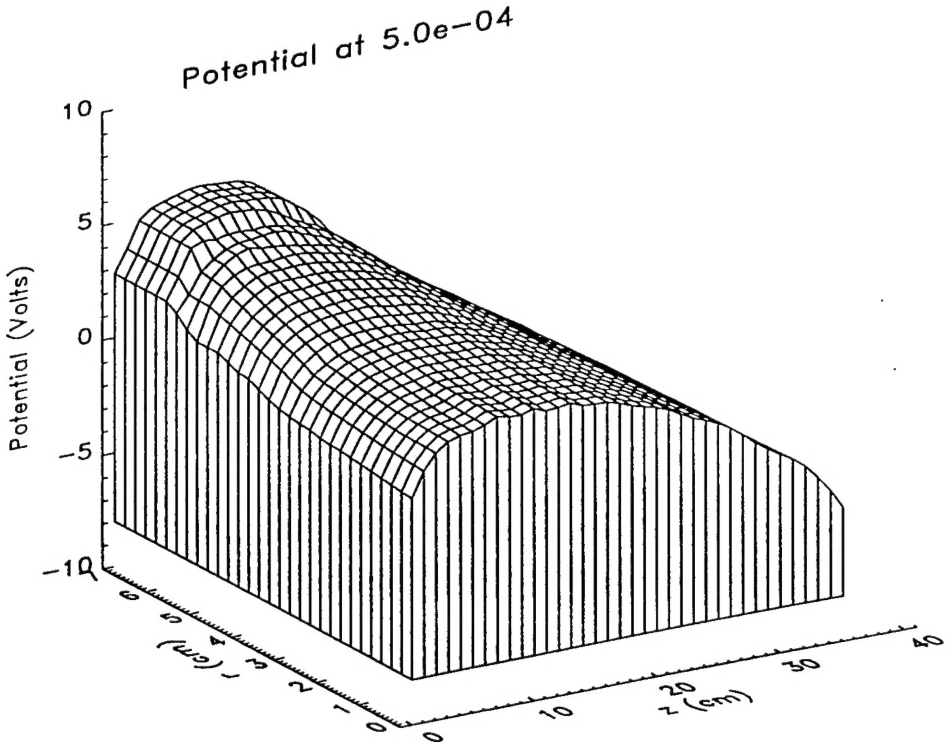

(a)

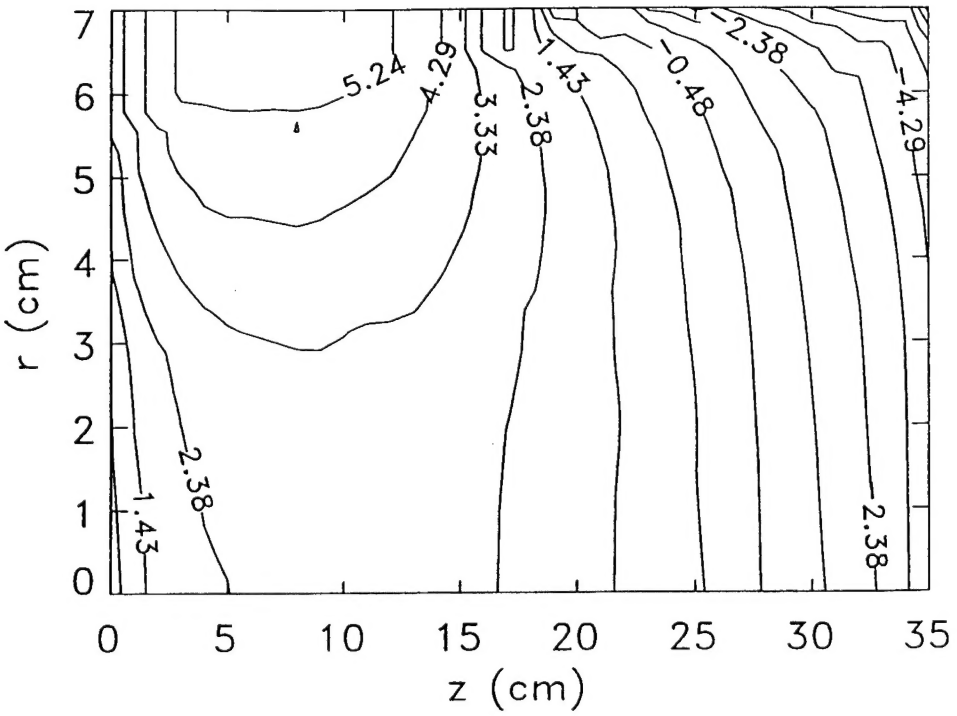

(b)

Fig. 10 — Plasma potential $\phi(r,z)$ from the simulation of Fig. 5 at time 500 μsec, shown as a surface plot (a) and a contour plot (b).